

Distances, Radial Distribution and Total Number of Galactic Supernova Remnants

S. RANASINGHE¹ AND D. LEAHY¹

¹*Department of Physics and Astronomy, University of Calgary, 2500 University Dr NW, Calgary, AB, T2N 1N4, Canada*

ABSTRACT

We present a table of 215 SNRs with distances. New distances are found to SNR G51.26 + 0.11 of 6.6 ± 1.7 kpc using HI absorption spectra and to 5 other SNRs using maser/molecular cloud associations. We recalculate the distances and errors to all SNRs using a consistent rotation curve and provide errors where they were not previously estimated. This results in a significant distance revisions for 20 SNRs. Because of observational constraints and selection effects, there is an apparent deficit of observed number of Galactic supernova remnants (SNRs). To investigate this, we employ two methods. The first method applies correction factors for the selection effects to derive the radial density distribution. The second method compares functional forms for the SNR surface density and selection function against the data to find which functions are consistent with the data. The total number of SNRs in the Galaxy is ~ 3500 (Method 1) or in the range ~ 2400 to ~ 5600 (Method 2). We conclude that the current observed number of SNRs is not yet complete enough to give a well-determined total SNR number or radial density function.

Keywords: Supernova Remnants(1667) — Radio astronomy(1338) — H I line emission(690) — Galaxy structure(622)

1. INTRODUCTION

Supernova remnants (SNRs) are an important area of study, as they give insight into the evolution of the interstellar medium (ISM) and galaxies. To better understand our galaxy, not only the study of individual SNRs is important but also an accurate count of Galactic SNRs is essential. Currently there are 294 known Galactic SNRs (Green 2019) and there is an apparent deficit between the number of observed and expected Galactic SNRs based on supernovae rates.

If the Supernova (SN) rate of the Milky way galaxy is one per 40 ± 10 yr (Tammann et al. 1994) and we assume the mean lifetime of radio SNRs to be $\sim 60,000$ yr (Frail et al. 1994a), the expected number of Galactic SNRs is of order 1500. This leaves the majority of SNRs yet to be discovered. The probable reason for the deficit is that the surveys searching for radio SNRs have selection effects (Green 1991; Case & Bhattacharya 1998). Mainly they overlook faint SNRs as well as young compact SNRs due to the limitations on resolution and sensitivity. Identifying large faint remnants remains a difficult task because of their low surface brightness and complex structure.

Identifying young compact SNRs is challenging as well, since they lack a shell-like morphology and are dif-

ficult to distinguish from extragalactic sources. Based on both statistics of known Galactic SNRs and SN rate, Ranasinghe et al. (2021) stated the expected number of young compact SNRs in our galaxy is $\sim 15 - 20$. They found 2 compact SNRs in the region covered by the THOR survey (Beuther et al. 2016; Wang et al. 2020), which was half the expected value. However, this number was found to be consistent with the THOR sensitivity limit. Even with a liberal estimate for these compact SNRs, it falls short to compensate for the deficit.

The main goal of this work is to examine the radial distribution of Galactic SNRs and the affect of observational selection effects. To this end we employ two methods. First, we use a simple empirical method for the correction of observational selection effects as previously investigated by Kodaira (1974) & Leahy & Wu (1989) with a smaller sample. The second method uses fitting of functional forms to the observed data to obtain functions that best describe the radial distribution.

In order to investigate the radial distribution of Galactic SNRs, accurate distance estimates for the SNRs are crucial. There are a considerable number of SNRs that have distances estimated using the Σ -D relation (surface brightness (Σ)- physical diameter (D) relation). However, there is a large scatter in the Σ -D distribution for Galactic SNRs and the physical diameter varies by

about an order of magnitude (Green 1991, 2005). Hence, for this work we utilize distances obtained by more reliable methods (e.g. HI absorption spectra and molecular cloud (MC) interactions).

In Section 2, the compilation of the SNR distances are presented. Description of the two methods used to estimate the SNR surface density distribution and their results are given in Section 3. The discussion and conclusion are presented in Sections 4 & 5, respectively.

2. COMPILATION OF SNR DISTANCES

To obtain the source list, we use the catalogue presented by Green (2019)¹. Apart from this catalogue, we use the catalogue presented by Ferrand & Safi-Harb (2012)² to search for remnants with reliable distances. Furthermore, we performed a literature search for newly identified SNRs.

For SNRs with no published distances, if there are molecular cloud or maser associations, we infer the distances from those. The literature distances have been estimated using different rotation curves, where the distance to the Galactic center (GC), R_0 ranging from 7.6 to 8.5 kpc and the orbital velocity of the Sun, V_0 ranging from 200 to 245 km s⁻¹. In this work, for consistency we recalculate the distances using the values presented by Reid et al. (2014) of $R_0 = 8.34 \pm 0.16$ and $V_0 = 241 \pm 8$ km s⁻¹ along with their “Univ” parameters to estimate a distance where an associated velocity is given. The errors of the distances were recalculated as described by Ranasinghe & Leahy (2018a).

2.1. Distances to Galactic SNRs

Green (2019) gives the current number of Galactic SNRs as 294 while the catalogue presented by Ferrand & Safi-Harb (2012) gives the current number as 383. These 383 SNRs include uncertain SNRs and candidate SNRs in Green (2019). The uncertain SNRs need further observations to confirm their nature and we include them in this study, while the SNR candidates are not. Many studies have produced SNR candidates (e.g. Anderson et al. (2017), Hurley-Walker et al. (2019)). However, some of these candidates may not be SNRs and add contamination to the sample of SNRs. Therefore, as a caution we exclude them from this study.

Out of the 294 SNRs in Green’s catalogue, 192 SNRs have distances estimated using reliable methods. The list of the sources is given in Table 1 with revised distances where relevant. There are 17 uncertain SNRs with distances that are found in the catalogue presented

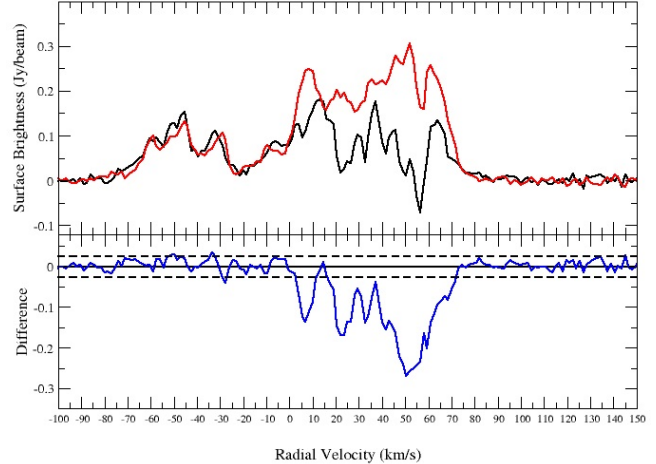


Figure 1. HI spectrum of the SNR G51.26 + 0.11. Top: HI emission spectra (source: black; background: red). Bottom: source – background difference: (blue). The $\pm 2\sigma$ noise level of the difference is shown by the dashed lines.

by Ferrand & Safi-Harb (2012) (Table 1 sources with †).

Furthermore, a literature search produced 6 newly identified SNRs (Table 1 sources with ‡), bringing the total number of sources in this sample to 215.

2.1.1. New Distance Estimate for SNR G51.26 + 0.11

G51.21 + 0.11 was given as a SNR candidate by Anderson et al. (2017). With a $\sim 11.3'$ radius, it is located 30' from the SNR G51.04 + 0.07 and reclassified as G51.26 + 0.11 by Dokara et al. (2018).

The HI spectra for the SNR G51.21 + 0.11 were constructed with data from the THOR data release 2 (Wang et al. 2020).

Examination of the HI spectra (Figure 1 and individual HI channel maps, shows absorption up to the tangent point (~ 70 km s⁻¹ or 5.2 kpc). Therefore, the SNR is located beyond the tangent point. HI channel maps do not show absorption at 15 or 37 km s⁻¹. Because we do not see absorption at 37 km s⁻¹, the upper limit is the corresponding distance of 7.7 kpc. We place the SNR at a distance of 6.6 ± 1.7 kpc.

2.2. Revised Distances to SNRs

The revised distance estimates of SNRs were done using a consistent rotation curve (Reid et al. 2014) throughout this work. We present the distance estimates for one SNR (G5.5 + 0.3) with a MC association and four SNRs (G341.9 – 0.3, G342.0 – 0.2, G343.1 – 0.7 and G354.8 – 0.8) with maser associations. The analyses of the distances to 9 SNRs were re-done with a combination of either new information or evidence. These distance estimates are a significant improvement from previously known values. The positions of the Galactic

¹ <http://www.mrao.cam.ac.uk/surveys/snrs/>

² <http://www.physics.umanitoba.ca/snr/SNRcat>

SNRs shown in figure 2 includes the revised distances from Table 2

G5.5+0.3: There were no previous distance estimated for this SNR. Liszt (2009) suggested a possible CO association with the SNR at $10 - 15 \text{ km s}^{-1}$. We take the average 12.5 km s^{-1} to estimate the near distance of $3.2 \pm 0.7 \text{ kpc}$, consistent with Liszt (2009).

G11.2 – 0.3: For SNR 11.2 – 0.3, the HI absorption spectrum was shown by Becker et al. (1985). With no HI absorption up to the tangent point, Green (2004) recalculated the distance to be 4.4 kpc. However, Kilpatrick et al. (2016) reported velocity-broadened molecular emission toward the remnant at an average of 32.5 km s^{-1} . This is consistent with the HI data and we place the SNR at the near distance of $3.7 \pm 0.2 \text{ kpc}$.

G53.6 – 2.2: From HI observations Giacani et al. (1998) adopted a systematic velocity of $+27 \text{ km s}^{-1}$ for the SNR but favoured the near kinematic distance $2.3 \pm 0.8 \text{ kpc}$. However, Shan et al. (2018) using the optical extinction - distance relation obtained a distance lower limit of 5.3 kpc. We place the SNR at the far distance of $7.8 \pm 0.6 \text{ kpc}$.

G311.5 – 0.3: Caswell et al. (1975) analysed HI absorption to place the SNR at $d > 6.6 \text{ kpc}$. Examination of their spectrum (their Figure 6), shos that at -10 km s^{-1} there is no absorption, rather clear absorption at $\sim 0 \text{ km s}^{-1}$. Therefore, we place the SNR at the far distance of $10.3 \pm 0.5 \text{ kpc}$ which corresponds to the velocity of -10 km s^{-1} .

G312.4 – 0.4: Doherty et al. (2003) presented HI absorption spectra for the SNR and gave a lower limit distance of 6 kpc. The tangent point velocity in this direction is $\sim -65 \text{ km s}^{-1}$. Comparing the point source spectrum and the SNR HI absorption spectrum (their Figure 7 & 8), the SNR absorption doesn't show up to the tangent point (the point source shows absorption up to the tangent point). We believe it's likely that the SNR is located at a distance of 3.5 kpc corresponding to -50 km s^{-1} .

G316.3 + 0.0: The HI absorption spectrum presented by Caswell et al. (1975) (their Figure 9) clearly indicates absorption up to the tangent point. The SNR lies beyond the corresponding distance of 6 kpc. However, there is no absorption present at $\sim -40 \text{ km s}^{-1}$ which leads to the conclusion that the SNR is located at less than the corresponding distance. Therefore, we place the SNR at a distance of $9.4 \pm 0.4 \text{ kpc}$.

G337.2–0.7: Rakowski et al. (2006) reported the SNR lies between a distance of 2.0 ± 0.5 and $9.3 \pm 0.3 \text{ kpc}$. Their Figure 4 shows the absorption spectra for the HII region G337.1 – 0.2 and the SNR, with both objects

showing absorption up to -116 km s^{-1} . This is the tangent point velocity and because the HII region is located at a distance of 11 kpc (Corbel et al. 1999), the SNR must be located beyond the tangent point. Examining both spectra, it is seen that the HII region shows absorption at -100 km s^{-1} while the SNR does not. We believe the SNR is located nearer than the HII region at a distance of 9.4 ± 0.3 corresponding to the velocity of -100 km s^{-1} .

G338.3 + 0.0: Supan et al. (2016) utilized HI absorption and ^{12}CO emission spectra to find a distance of either 8.5 or 13 kpc. The tangent point velocity corresponding to the rotation curve of Reid et al. (2014) is $\sim 120 \text{ km s}^{-1}$. The Supan et al. (2016) HI absorption spectra show absorption up to the tangent point. Thus, we resolve the kinematic distance ambiguity and place the SNR at distance of 13 ± 0.4 corresponding to a velocity of -31 km s^{-1} .

The SNRs G341.9 – 0.3, G342.0 – 0.2 and G343.1 – 0.7 have no previously estimated distances. However, Koralesky et al. (1998) detected OH masers towards the remnants and we use their LSR velocity to estimate the distances. This places the SNRs G341.9 – 0.3 and G342.0 – 0.2 at a distance of $15.8 \pm 0.6 \text{ kpc}$. For G343.1 – 0.7, $v_{\text{LSR}} = -70 \text{ km s}^{-1}$ and which yields the near distance of $4.9 \pm 0.2 \text{ kpc}$.

The distance to the SNR G346.6 – 0.2 was presented by Koralesky et al. (1998) as either the near distance of 5.5 kpc or the far distance of 11 kpc corresponding to a radial velocity of 76.0 km s^{-1} . Auchettl et al. (2017) used the tangent point distance of 8.3 kpc in their XMM-Newton study. We adopt the far distance of $10.4 \pm 0.2 \text{ kpc}$ consistent with Auchettl et al. (2017).

G348.5+0.0: Tian & Leahy (2012) presented an upper limit to the distance to the remnant as 6.3 kpc. With HI absorption not present at -107 km s^{-1} , the corresponding distance would be an upper limit (7.8 kpc with the rotation curve parameters presented by Reid et al. (2014)). The OH maser toward the SNR at -100 km s^{-1} (Koralesky et al. 1998) places the SNR is at a distance of $7.2 \pm 0.2 \text{ kpc}$.

G354.8 – 0.8: The SNR has no previously known distance. We use the OH maser towards the SNR reported by Koralesky et al. (1998) at $v_{\text{LSR}} = -70 \text{ km s}^{-1}$ to estimate the distance to the SNR. The kinematic distance ambiguity for the SNR cannot resolved and the distances are either 7.7 ± 0.2 or $8.9 \pm 0.2 \text{ kpc}$. We take the average to place the SNR at a distance of $8.3 \pm 0.8 \text{ kpc}$.

3. RADIAL DISTRIBUTION AND TOTAL NUMBER OF GALACTIC SNRS

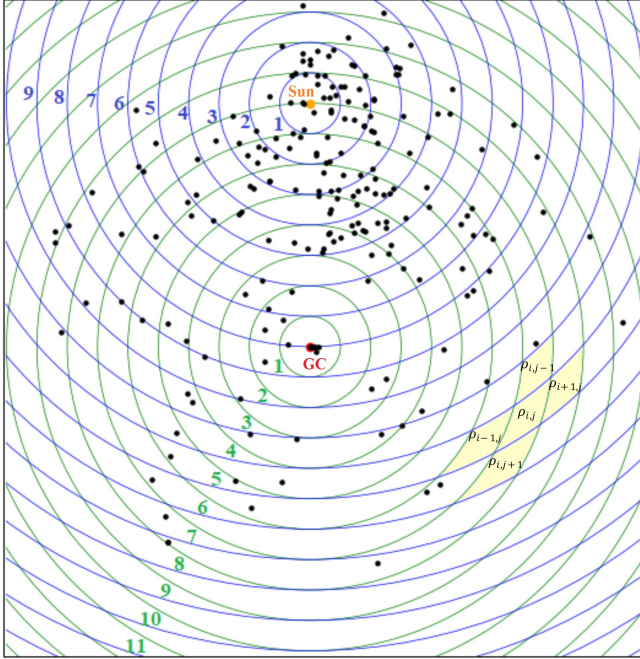


Figure 2. Positions of Galactic SNRs from Table 1 projected onto the Galactic plane. The black dots show the positions of the SNRs. The concentric green rings (i : numbered in green) are at radii multiples of 1.0425 kpc centred at the Galactic center (GC; red circle) and the blue rings (j : numbered in blue) are at radii multiples of 1.0425 kpc centred at the Sun (yellow circle). The yellow shaded regions show examples of the label system.

Detection of SNRs in the Galaxy is difficult because they are extended objects and the Galaxy has a diffuse synchrotron background and large number of HII regions which emit at the same radio frequencies as SNRs. Another reason is that SNRs can be similar or lower surface brightness than the background and confusing sources. Thus radio observations only detect some fraction of all SNRs in the Galaxy. This effect of detecting only a fraction of the SNRs is known as selection effects. We can account for selection effects in two ways: empirically defining correction factors which are the inverse of the selection function (which is less than 1); or as a functional form of the selection function. We refer to these two methods as Method 1 and Method 2.

3.1. Method 1

For Method 1, to determine the true surface densities we make the following assumptions:

1. The underlying surface density of SNRs is circularly symmetric about the GC;
2. The underlying density is symmetric about line joining GC and Sun (R_0);

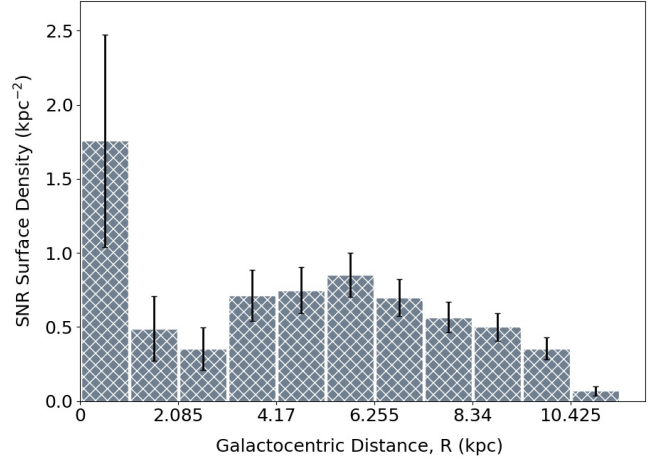


Figure 3. The observed Galactic SNR densities (uncorrected).

3. The correction factors depend only on distance from the Sun (d).

Due to observational selection effects, SNRs are concentrated near the Sun. Figure 2 shows the projection of the known Galactic SNRs with distances on the Galactic plane. The concentric circles around the GC and Sun (Figure 2 green and blue circles, respectively) were constructed with radii in multiples of $R_0/8$. The regions of interest are the smaller regions bound by the lines. We adopt the distance to the Sun (R_0) as 8.34 kpc (Reid et al. 2014).

3.1.1. Determination of Correction Factors and Surface Densities

To determine the the surface densities we first smooth the observed densities. Because the densities vary smoothly with R and d , the 2-dimensional smoothing is done using

$$\rho'_{i,j} = (\rho_{i,j-1} + \rho_{i-1,j} + 4\rho_{i,j} + \rho_{i,j+1} + \rho_{i+1,j})/8. \quad (1)$$

Here ρ' is the smoothed surface density and i & j (green and blue numbered rings in Figure 2) correspond to the circles from the GC (R) and Sun (d), respectively (Leahy & Wu 1989). An example of the labelling is shown in Figure 2 (yellow shaded regions).

However, equation (1) is valid only for the regions that exclude the regions intersecting the extended Sun-GC line. There are 6 regions surrounding each region for the regions intersecting the extended Sun-GC line except for the regions where the Sun and GC are enclosed by the first ring ($i = 1$ and $j = 1$, respectively). For the regions with 6 surrounding regions, we smooth the densities with

the relation

$$\rho'_{i,j} = (\rho_{i-1,j+1} + \rho_{L:i,j+1} + \rho_{R:i,j+1} + 6\rho_{i,j} + \rho_{L:i+1,j} + \rho_{R:i+1,j} + \rho_{i+1,j-1})/12. \quad (2)$$

The regions, excluding those intersecting the extended Sun-GC line, have mirror counterparts with the same i & j indices. Therefore, in equation (2) we denote the left and right regions with L and R subscripts.

Finally, the four regions where the Sun and GC enclosed by the first ring (the regions: $\rho_{1,8}$, $\rho_{1,9}$, $\rho_{8,1}$ & $\rho_{9,1}$) have only four regions surrounding them. The smoothing of these regions is done similar to the other regions with equation (1).

Next, the correction factors for the smaller regions are calculated. The correction factor (C) for a region in a particular ring is the density of the region in the line between the Sun and GC divided by the average density of the region of interest and its mirror counterpart. For an example, $C_{4,7} = \rho'_{4,5}/(\rho'_{L:4,7}/2 + R\rho'_{R:4,7}/2)$. This yields the correction factors for all regions except the regions in the line connecting the sun and the GC.

For the $i = 1$ ring, we simply take the correction factor for $\rho_{1,8}$ region to be $\rho_{1,8}/\rho_{1,9}$. Furthermore, we assume no correction is factor is needed for the $j = 1$ ring. The assumption here is within ~ 1 kpc radius of the Sun, observations are not affected by the selection bias. The rest of the correction factors (regions intersecting the sun-GC line) are taken to be the same as for the region at same d but next larger R (if $R < R_0$) or next smaller R (if $R > R_0$). Because the regions in a ring are not equal to each other, the weighted average surface density of a each ring is calculated.

To estimate the error in each ring, we take the standard error (SE) using the corrected surface densities of all regions in that ring. The standard error is calculated using $SE = \sigma_s/\sqrt{n}$, where σ_s is the sample standard deviation and n the number of regions. For the $i = 1$ ring, the uncorrected densities were used for the error estimate.

3.1.2. Surface Density and Estimate of the Total Number of SNRs

The densities and estimated numbers of SNRs from Method 1 are given in Table 2. From this work, there are now 215 SNRs with known distances (Table 1). We have excluded SNRs with distances that are given only as a lower or upper limit. There are no SNRs between 12.51 and 15.6375 kpc. All SNRs in this sample except three are located at distances of less than ~ 11.5 kpc from the GC. For the three exception, G306.3 – 0.9 is

Table 2. SNR Surface Density Estimates from Method 1

R ^a (kpc)	SNR Densities (kpc ⁻²)	# of SNRs
0 – 1.0425	2.12 ± 0.78	7 ± 3
1.0425 – 2.085	0.79 ± 0.32	8 ± 3
2.085 – 3.1275	0.97 ± 0.14	16 ± 2
3.1275 – 4.17	2.34 ± 0.41	56 ± 10
4.17 – 5.2125	2.35 ± 0.29	72 ± 9
5.2125 – 6.255	3.02 ± 0.37	113 ± 14
6.255 – 7.2975	2.96 ± 0.26	131 ± 11
7.2975 – 8.34	5.52 ± 0.61	283 ± 31
8.34 – 9.3825	3.44 ± 0.48	200 ± 28
9.3825 – 10.425	1.91 ± 0.38	124 ± 25
10.425 – 11.4675	0.56 ± 0.12	40 ± 9
Total		1050 ± 145

NOTE—a: The galactocentric distances R are multiples of $R_0/8 = 1.0425$ kpc.

located at a galactocentric distance (R) of 16.5 kpc, G184.6 – 5.8 is at 11.7 kpc and G141.2 + 5.0 is at 11.7 kpc. G306.3 – 0.9 is the only SNR in its corresponding ring, so we exclude that ring from this analysis (because we do not expect to obtain a reasonable surface density, i.e. $\rho \sim 0$ kpc⁻²). For the same reason, G141.2 + 5.0 and G184.6 – 5.8 were excluded from this analysis leaving 206 SNRs in the sample.

The SNR surface densities estimated in Method 1 only extend up to a galactocentric distance $R \simeq 11.5$ kpc. In reality the surface densities are expected to extend to a considerably further indicating an incomplete sample. Therefore, the Method 1 estimated number of SNRs of 1050 ± 145 is only a lower limit. Figure 5 shows the corrected observed distribution of SNR surface densities (top panel) and the number of SNRs at each galactocentric distance R (bottom panel).

3.2. Method 2

To determine the true distribution of SNRs in our Galaxy, we assume circular symmetry of true SNR density about Galactic center (R) and that the selection function only depend on distance from the Sun (d) and Galactic longitude (l). In this case we use a functional form ($f_{sel}(d, l)$) that represents the selection effects.

3.2.1. Fitting the Galactic SNR Distribution with Functional Forms

The first step is to bin the SNRs in Galactic x and y, with each bin on a square grid on the Galactic plane centred on the Galactic center and 1.0425×1.0425 kpc ($R_0/8$) in size (see Figure 8 for the grid). The total number of bins is 400 (20×20). Then the functional forms for the surface density, $\rho_{SNR}(R)$ and for the correction function $f_{sel}(d, l)$ were chosen. For the SNR surface density, $\rho_{SNR}(R)$ we select from the following set:

1. Exponential distribution (Exp) with scale length H_r ,

$$\rho_{SNR}(R) = \exp\left(-\frac{R}{H_r}\right).$$

2. Power-law distribution with core (PL_C) where core radius R_c and α_1 are fitting parameters,

$$\rho_{SNR}(R) = \left(1 + \frac{R}{R_c}\right)^{-\alpha_1}.$$

3. Gaussian distribution (GD) with a mean μ and standard deviation σ ,

$$\rho_{SNR}(R) = \exp\left(\frac{-(R - \mu)^2}{2\sigma^2}\right).$$

4. Modified gamma function (MGF; [Stecker & Jones 1977](#); [Case & Bhattacharya 1998](#); [Verberne & Vink 2021](#)),

$$\rho_{SNR}(R) = \left(\frac{R}{R_0}\right)^{\alpha_1} \exp\left(-\beta \frac{R - R_0}{R_0}\right).$$

5. Distribution with a non-zero surface density at the GC ([Case & Bhattacharya 1998](#) equation 15, hereafter referred to as CB98e15),

$$\rho_{SNR}(R) = \sin\left(\frac{\pi R}{R_a} + \theta_0\right) e^{-\beta R}.$$

6. Sérsic (1963) profile,

$$\rho_{SNR}(R) = \exp\left(-b_n \left[\left(\frac{R}{R_e}\right)^{1/n} - 1\right]\right).$$

For Sérsic function, n and the half-light radius, R_e are free parameters. There are a few approximations for the constant b_n (see [Graham & Driver \(2005\)](#)) in terms of the parameter n for $n > 0.36$ ([Ciotti & Bertin 1999](#)). However, because the range of n is unknown, we obtain b_n by solving the equation $\Gamma(2n) = 2\gamma(2n, b_n)$. Here Γ is the (complete) gamma function and γ is the lower incomplete gamma function ([Ciotti 1991](#)).

For the correction function $f_{sel}(d, l)$, one of the following forms were chosen:

1. Exponential distribution (Exp) with scale length H_s ,

$$f_{sel}(d, l) = \exp\left(-\frac{d}{H_s}\right) (1 + B \cos(l - l_0)).$$

2. Power-law distribution with core (PL_C),

$$f_{sel}(d, l) = \left(1 + \frac{d}{R_s}\right)^{-\alpha_2} (1 + B \cos(l - l_0)),$$

with R_s , l_0 , B and α_2 fitting parameters. There are two main contributing factors to the selection effects: 1) Difficulty in detection of SNRs where the Galactic synchrotron background is bright, 2) The sensitivity of observations/surveys in various regions of the Galactic plane. Therefore, a simple function was chosen to represent the Galactic synchrotron and sparseness of the data, a two-term Fourier series $(1 + B \cos(l - l_0))$. A simpler function (i.e. just the constant) does not describe the data well (see section 4.3).

The model is the product of $\rho_{SNR}(R)$ and $f_{sel}(d, l)$. This is fit to the observed distribution using χ^2 minimization. The χ^2 function is given by

$$\chi^2 = \sum_{i=1}^N \frac{(N_i - n_i)^2}{\sigma_i^2}.$$

Here N_i is the observed number of SNRs in each bin, n_i is the model number of counts and σ_i is the error of the observed counts.

Because a significant number of bins are empty ($N_i = 0$) or have a small number of counts ($N_i \lesssim 10$), we use the Y^2 statistics as described by [Lucy \(2000\)](#) where

$$Y^2 = \nu + \sqrt{\frac{2\nu}{2\nu + \sum_i n_i^{-1}} (\chi^2 - \nu)}$$

and ν is the number of degrees of freedom ([Press et al. 2007](#)). The errors for all the fitting parameters were found by finding the minimized Y^2 while keeping all parameters constant except for the parameter of interest.

3.2.2. SNR Surface Densities and Correction Functions from Method 2

The model parameters for the observed SNR densities were found by performing a Y^2 statistic minimization and are given in Table 3. The parameter errors were calculated by fixing the minimized Y^2 at $+1\sigma$ and by calculating individual errors. Therefore, the true parameter errors are likely larger than the 1σ error.

All models give good results except for case of the SNR density is a power-law distribution with R_c and α_1 left

as free parameters. Here the parameters, R_c and α_1 are degenerate and provide equally good Y^2 values for large parameter values. Thus, we set the power-law exponent $\alpha_1 = 2$ and 1.5 in two cases, which yield the Plummer sphere and the Kuzman disk, respectively, (Sparke & Gallagher 2007).

For the SNR surface density as a Gaussian distribution, we left the mean as a free parameter or fixed at $R = 0$ kpc. Both distributions yield a low Y^2 value and are included in Table 3.

Each model (product of surface density and selection function) has been superimposed on the observed SNR surface densities in Figure 8. The differences in Y^2 statistic between all models shown are $\lesssim 2\sigma$. Therefore, we do not favour one model over another simply on the basis of the Y^2 statistic.

4. DISCUSSION

4.1. Distance Estimates

We compiled 215 SNRs with distances. Out of these we find distances to 6 SNRs where distances were previously unknown. A distance of 6.6 ± 1.7 kpc was determined for the SNR G51.21 + 0.11 using HI absorption, and the distances to the other five SNRs (G5.5 + 0.3, G341.9 – 0.3, G342.0 – 0.2, G343.1 – 0.7 and G354.8 – 0.8) were determined by MC/maser associations.

Distances to 135 of the SNRs are unchanged from the most recent literature values. These distances were obtained using HI absorption spectra, HI data analysis, maser and MC associations along with the Reid et al. (2014) rotation curve or by other methods (pulsar associations, parallax measurements etc.), where the radial velocity of the SNRs were unknown.

We have revised the distances or added new errors to 74 SNRs. The 74 SNRs include 9 distances that were significantly revised (see Section 2.1). The distances for 20 of the 73 SNRs were improved at least by 10%. For 7 SNRs, we find the distances to be consistent with the literature values but present new estimates for errors. The distances to 38 SNRs slightly differ from the literature values due to the use of different rotation curves. Out of the the 38 SNRs, 15 did not have previously estimated errors. The 5 SNRs located near the GC do not have previously estimated errors (Table 1). Due to the somewhat uncertain nature of their locations, we do not consider the errors to be accurate. For their errors, we utilize the error in R_0 of ± 0.16 kpc presented by Reid et al. (2014).

Pihlström et al. (2014) places the SNR G1.4 – 0.1 near the GC. While we included this SNR in our sample given in Table 1, we exclude from further analysis due to lack of strong evidence for its distance.

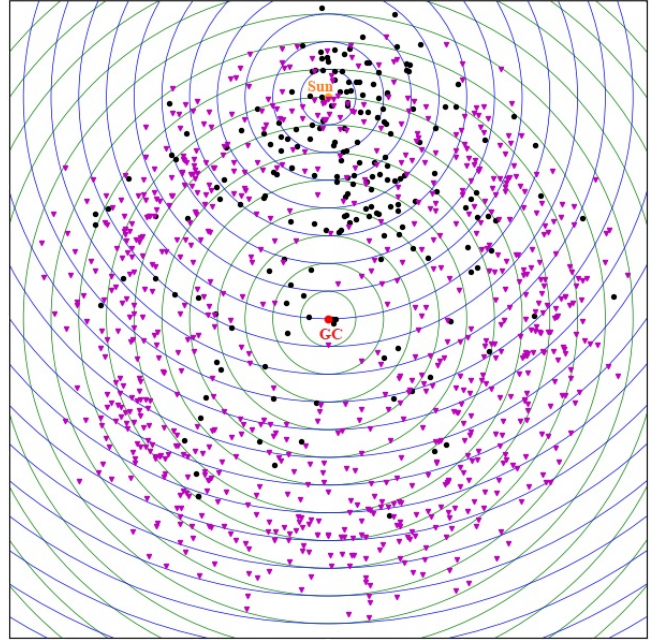


Figure 4. The black circles are the positions of observed SNRs and the violet triangles are positions a simulated set of 1050 SNRs (Method 1). The ring radii are in multiples of 1.0425 kpc.

4.2. The Estimated Surface Density Using Method 1

With the SNR surface densities, total number of SNRs in the Galaxy ($R \lesssim 11.5$ kpc) can be estimated. Figure 4 shows the predicted number of SNRs (from Method 1) placed randomly in each Galactic ring. There is a low density of SNRs for $R \lesssim 3$ kpc.

Figure 5 top panel shows SNR surface density distribution from Method 1. The red dashed line is the best-fit straight line for all bins with $R < 9$ kpc. Figure 3 shows the uncorrected densities for comparison.

The best-fit line when excluding the low densities in bins $1.0425 < R < 3.1275$ kpc is green solid line in Figure 5. The best-fit line excluding the first 3 bins, (violet dot-dash line) is nearly the same. Both shows interpolated densities for the excluded region of $1.0425 < R < 3.1275$ kpc to be 2–3 times as large as the derived model densities. The latter two linear fits predicts an additional ~ 25 SNRs in this region. A low density in the $1 < R < 3$ kpc region might be expected. The majority (about 85%; Tammann et al. 1994) of the SNe are core-collapse (CC), where the progenitor is a young massive star ($> 8M_{\odot}$). The deficit of observed star forming regions or high mass X-ray binaries at Galactocentric distance, $R \lesssim 3$ kpc (Russeil 2003; Bodaghee et al. 2012) is consistent with the low density of SNRs in this region. The Method 1 SNR distribution seem to be consistent with the distribution of star form-

ing complexes presented by (Russeil 2003). Similar to these complexes, the observed SNR distribution does not show any large scale spiral structure. The low density of HII regions at a Galactocentric radius, $R < 3.5$ kpc is evident from the observations made by Lockman (1981), Anderson & Bania (2009) and Anderson et al. (2012). Additionally, the low density of Galactic young objects and masers at $R \lesssim 3$ was apparent in the study done by Shen & Zheng (2020) on the Galactic structure.

Even though the majority of SNe are CC, the contribution of the SNRs resulted by type Ia explosions is significant. The distribution of type Ia SNRs in the Galaxy would not follow the distribution of star forming regions. It is possible that the majority of SNRs in the region $R \lesssim 3$ kpc are type Ia. In fact, of the 215 SNRs in our sample, 16 SNRs lie in the region $R \lesssim 3$ kpc and SN types of 8 of these are known. 3 SNRs of the 8 are CC and 5 are type Ia. While the sample here is too small to form a definite conclusion, the observations are consistent with the deficit of CC SNRs in the region $R \lesssim 3$ kpc.

As a test for the Method 1 validity, we have conducted simulations to estimate the SNR density distribution. For a chosen initial number of SNRs, we placed them in each ring (i^{th} ring; Figure 2) consistent with a surface density distribution that is combined with a correction function (see Section 3.2). From the resultant distributions (simulated observed SNR distribution), we estimated the surface density distributions using Method 1. These tests have shown that the smoothing and corrections produce a total number of SNRs that is less than the initial input ($\sim 1/3.5$). The Method 1 SNR surface density estimations are sensitive to slight changes and the sparseness of the data leads to an underestimation of the total number of Galactic SNRs. Therefore, the total number of Galactic SNRs (1050) estimated using Method 1 is likely a lower limit and the total number of SNRs is estimated at roughly as ~ 3500 .

4.3. Estimated Surface Densities Using Method 2

The models and best-fit parameters for the surface density and correction functions are given in Table 3. For all models shown³, the Y^2 statistics show that the fits are equally good within 2σ . The contour maps in Figure 8 are of the product of SNR surface density functions and correction functions ($A\rho_{SNR}(R)f_{sel}(d, l)$). The numbers of observed SNRs are shown by the green 1.0425×1.0425 kpc grid. From Figure 8, it is seen that

³ We ran a number of other models of similar other functional forms with or same functional forms with fewer parameters- all of those models (not shown) had higher Y^2 by more than 2σ .

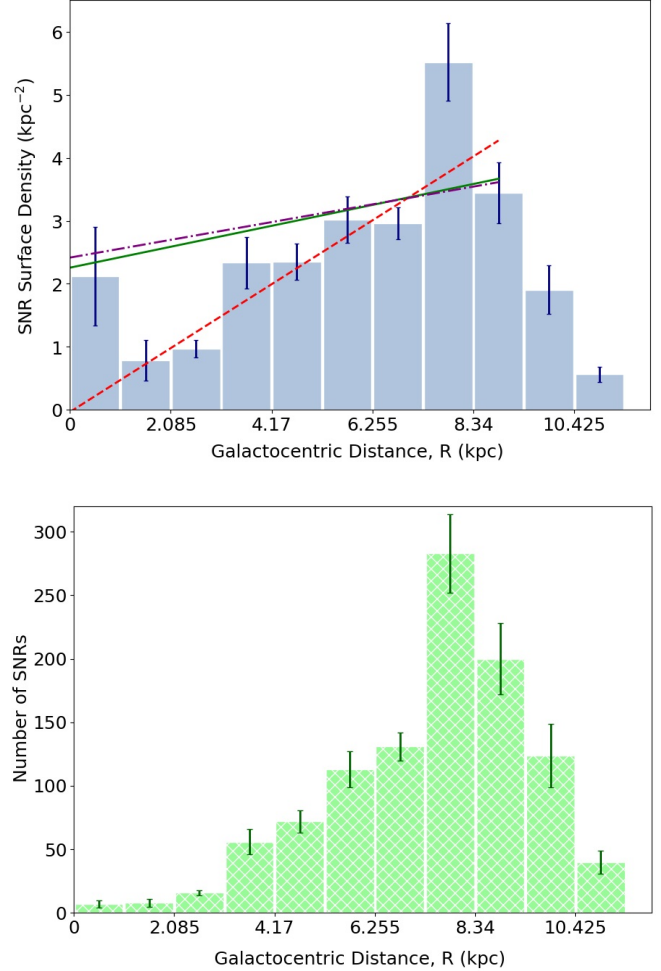


Figure 5. Top: the surface density distribution estimated from Method 1. The dashed red line is best-fit line to SNR surface densities < 9 kpc, the green solid line is the best-fit line omitting only the surface densities between 1.0425 and 3.1275 kpc and the violet dash-dot line omits the first three bins. Bottom: the distribution of the predicted total number of SNRs in each ring.

the model distributions appear to be in agreement with the observed distribution of SNRs.

The exponential profiles for the SNR surface density yield reasonable Y^2 values and scale lengths (R_H). The Galactic thin disk scale length given by (Bland-Hawthorn & Gerhard 2016) is 2.6 ± 0.5 kpc. If the scale length (R_H) is fixed in the exponential profiles (see models 1 and 2 in Table 3), the resulting Y^2 values are 167.21 and 166.83 for the two selection functions, respectively. These Y^2 values are $< 1\sigma$ and $< 1.3\sigma$ higher than the model 1 and 2 values (Table 3), indicating that the scale lengths are consistent with the Galactic thin disk scale length. However, the SNR density functions significantly vary from each other, implying that the data is insufficient to differentiate between the listed models.

Figure 7 shows the radial distributions of the GD, $GD_{\mu=0}$, MGF, CB98e15 and Sérsic profiles. The MGF densities peak at $R = 4.1$ kpc and $R = 4.3$ kpc for the two correction functions (Exp and PL_C, respectively) and agree with the peak of the radial distribution (at $R \approx 5$ kpc) provided by Case & Bhattacharya (1998) within error.

The CB98e15 profile yields a non-zero density at the center and the parameters (see Table 3) are consistent with the parameters estimated by Case & Bhattacharya 1998. The density function is zero beyond $R = R_a(1 - \theta_0/\pi)$ ($R = 12.3$ and 12.5 kpc for exponential and power-law with core correction functional forms, respectively).

The parameter n that describes the shape of the Sérsic profile is low (~ 0.25) compared to common values of $n = 4$ & 1 (Ciotti & Bertin 1999). However, the half-light radius estimated in the Sérsic profile (R_e) of ~ 6 kpc is consistent with the expected value for a Milky way-like Galaxy (Chamba et al. 2020).

If we assume the observed SNRs for an area of $d \lesssim 1$ kpc are complete near the Sun, we find the SNR surface density to be 4.4 ± 1.1 kpc⁻². The model densities yield 5.1 to 6.1 kpc⁻² for the exponential correction function, whereas the power law correction function yields higher densities of 7.2 to 8.9 kpc⁻². These are higher than the observed density near the sun, indicating incompleteness by factor ~ 2 within 1 kpc of the sun (power law with core) or by factor ~ 105 (exponential).

Apart from the models provided in Table 3, we have investigated a few more complex models for the SNR surface density functional form. Among them, the sum of two Gaussian distributions and a distribution with a Galactic bar (Wegg et al. 2015) were tested. However, we found that the data was inadequate to determine best-fit parameters (the parameters are degenerate).

If the angular dependence is omitted, the models yield an increase in Y^2 value which is greater than 3σ and thus statistically significant, indicating the angular dependence of the correction function is necessary. We also tested the simplest model for the SNR surface density function: $\rho_{SNR}(R)$ is a constant. In this case, the parameters for the models ($Af_{sel}(d, l)$) are degenerate for both correction functions. The Y^2 values for both selection functions are ~ 172 and $> 2\sigma$ higher compared to the exponential density distributions (models 1 & 2). If the angular dependence is also ignored, the Y^2 values are higher by $> 3\sigma$ compared to models 1 and 2 in Table 3.

Therefore, with the current sample of SNRs, we conclude that more complex SNR surface density functions are not justified by the data, and that simpler functions

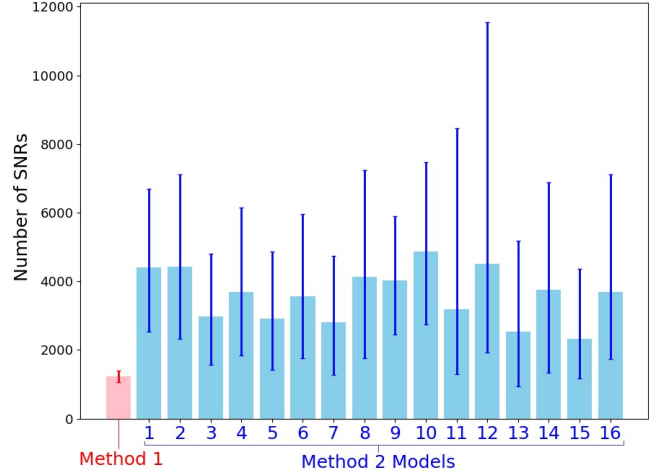


Figure 6. Total number of SNRs estimated using Method 1 (pink bar & red error) and Method 2 (light blue bars & blue errors). The Method 2 numbers correspond to the model numbers in Table 3. All numbers are calculated over the region $0 < R \leq 11.5$ kpc.

for SNR surface density or correction function are not allowed by the current data.

4.4. Comparison Between Method 1 and Method 2 Galactic SNR Surface Densities

Figure 6 shows the comparison of Method 1 SNR total number (pink bar) and Method 2 total SNR numbers (light blue bars), both integrated over the area of the Galaxy with $R \leq 11.5$ kpc. The CB98e15 and Sérsic profiles in the case that the correction function is an exponential distribution yield lower limit numbers of 940 and 1160 SNRs, respectively. While these are consistent with Method 1 number within error, the Method 2 density functions do not agree with the Method 1 densities.

Comparisons of the Method 2 density functions with each other and the Method 1 densities are shown in Figure 7. The Method 2 densities are consistent within errors (the error bands overlap) outside $R \sim 7$ kpc. The $GD_{\mu=0}$ density is inconsistent (higher than) the GD inside $R \sim 3.5$ kpc and higher than the other densities inside other R values, with R value dependent on the function. The exponential surface density (slightly higher than even the $GD_{\mu=0}$ density) is consistent with the Method 1 density only for a $R \gtrsim 8$ kpc and is similarly (like the $GD_{\mu=0}$ density) inconsistent with the other Method 2 densities in the inner Galaxy.

In summary, from Figure 2, we see that the observed number of SNRs is not complete and selection effects are clearly present. For Method 1, adding a few observed SNRs in a region where there are none, considerably increases (by $> \sim 0.1$ kpc⁻²) the smoothed and corrected densities. Figure 7 provides a summary of the results:

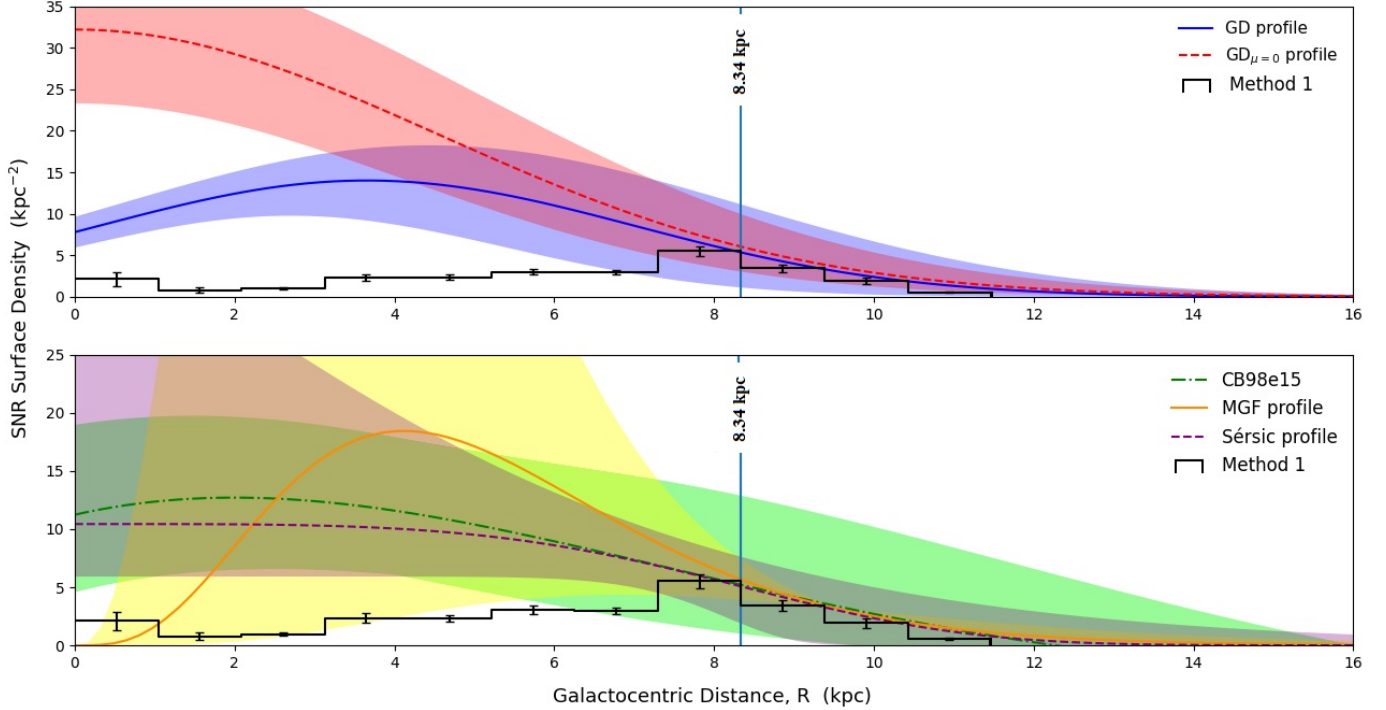


Figure 7. SNR surface densities from Method 2. Top: GD: blue solid curve and $GD_{\mu=0}$ profile: red dashed curve. Bottom: MGF: orange solid line, CB98e15: green dash-dot curve and Sérsic: purple dashed curve. All surface densities are for the case of an exponential correction function. The shaded regions are the lower and upper limits of the similarly-coloured profiles.

the current data results in density functions with large error bands, thus we conclude that identification of more observed SNRs is needed to constrain better Galactic SNR densities.

4.5. The Total Number of Galactic SNRs

While method 1 produced ~ 3500 total number of SNRs, Method 2 produced ~ 2400 to ~ 5600 SNRs. With ~ 300 observed Galactic SNRs (confirmed: Green (2019)), the majority of the SNRs remain to be discovered.

Using the THOR + VGPS combined survey, Anderson et al. (2017) presented 76 SNR candidates covered by the region between Galactic longitudes 17.5° and 67.4° and latitudes -1.25° and $+1.25^\circ$. Of the 294 SNRs there are only 52 SNRs in the region covered by THOR. If the Anderson et al. (2017) SNR candidates are confirmed, it brings the total Galactic SNRs in the region to 128 SNRs which is a $\sim 150\%$ increase.

Hurley-Walker et al. (2019) presented 27 SNR candidates using the GLEAM survey covered over Galactic longitudes, $345^\circ < l < 60^\circ$ and $180^\circ < l < 240^\circ$. Here 25 candidates are located at $345^\circ < l < 60^\circ$ and 2 are located at $180^\circ < l < 240^\circ$. Which increases the total numbers of SNRs if confirmed, by 17% and 22% respectively, for the two regions.

Considering both Anderson et al. (2017) and Hurley-

Walker et al. (2019) SNR candidates, an increase of 150% is a conservative estimate for $17.5^\circ < l < 67.4^\circ$ and extrapolating it to the Galaxy, if confirmed there may be as many as ~ 750 SNRs in the Galaxy. However, the total number of SNRs still fall short of the predicted number of a few thousand.

The majority of the SNRs are located in the Galactic plane. At least 90% of the 215 Galactic SNRs where distances are known (Table 1) are at a Galactic height, $z \lesssim 200$ pc. Most of the SNRs found in the Galactic plane are CC and can be associated with star forming regions. It is likely that many SNRs are not detected because of the confusion caused by objects (SNRs, star forming regions etc.) in the foreground.

The detection of faint SNRs depends on the sensitivity of observations/surveys. With increased sensitivity it is likely objects that are not associated with each other could be easily detected to lessen the confusion. However, the brightness of the foreground objects dominates in any particular region of the Galaxy and detection of the background objects would be a difficult task. Furthermore, SNRs will be difficult to detect where the Galactic synchrotron background is bright, which is mainly in the Galactic plane. While the predicted number of SNRs for the Galaxy is a few thousand, because of the above reasons the observations/detections of new SNRs could be limited to a few hundred.

5. CONCLUSION

In order to examine the distribution of Galactic SNRs, accurate distances are essential. Using HI absorption, we estimate the distance of 6.6 ± 1.7 kpc to the SNR G51.21 + 0.11, where the distance was previously unknown. Furthermore, using maser/MC associations, distances to five more SNRs where the distance were previously unknown were estimated. While distances to 135 SNRs remained unchanged, distances to 22 SNRs were significantly revised ($> 10\%$). We have produced a list of 215 Galactic SNRs with distances with enough accuracy to test models.

We utilized two methods in order to test density distributions for Galactic SNRs. Method 1 employs correction factors for the selection effects to derive a binned density. However, the density distribution estimated from this method is sensitive to slight changes. Because of the sparseness of the data and weaknesses

of the model, Method 1 yields only 1000 SNRs, while tests show this actual number may be closer to ~ 3500 Galactic SNRs

For the second method we test functional forms for the SNR surface density and the correction factor using fits to the observed data. Figure 7 shows the models are all consistent in the region near the sun but differ most near the Galactic center. The best-fit parameters for more complex models cannot be determined because of the limited sample size of observed SNRs.

Method 2 yields ~ 2400 to ~ 5600 SNRs.. The predictions for the total number of SNRs in the Galaxy are all > 1000 Additional observed SNRs are required to obtain results with small uncertainties for total number of SNRs and their radial distribution.

We thank Dr. B. Karchewski for helpful comments. This work was supported by a grant from the Natural Sciences and Engineering Research Council of Canada.

Table 1. Galactic SNRs with reliable distances

#	SNR ^a	Literature	Method	V_{LSR} (km s ⁻¹)	Ref	Revised	Galactocentric
		dist (kpc)				dist ^b (kpc)	dist (kpc)
1	G0.0 + 0.0	8	Galactic center	...	1	8.34 ± 0.16	0
2	G0.3 + 0.0	8.5	Galactic center	...	2	8.34 ± 0.16	0.04
3	G0.9 + 0.1	8.5	Galactic center	...	3	8.34 ± 0.16	0.13
4	G1.0 – 0.1	8	Galactic center	...	1	8.34 ± 0.16	0.15
5	G1.4 – 0.1	8.5	4
6	G1.9 + 0.3	8.5	Galactic center	...	5	8.34 ± 0.16	0.28
7	G4.5 + 6.8	$5.1^{+0.8}_{-0.7}$	Proper motion + v_{Shock}	...	6	...	$3.3^{+0.8}_{-0.7}$
8	G5.4 – 1.2	5.2	Kinematic distance	27	7,8	5.0 ± 0.3	3.4 ± 0.3
9	G5.5 + 0.3	12.5	9	3.2 ± 0.7	5.1 ± 0.7
10	G5.7 – 0.1 [‡]	2.9 ± 0.3	Optical extinction	12.8*	10	3.0 ± 0.7	5.3 ± 0.7
11	G6.4 – 0.1	1.9 ± 0.3	Kinematic distance	7	11	1.8 ± 0.3	6.6 ± 0.3
12	G7.5 – 1.7 [‡]	1.7	PWN association	...	12	...	6.7
13	G7.7 – 3.7	4.5 ± 1.5	Estimation (z distance)	...	13	...	3.9 ± 1.4
14	G8.3 + 0.0	16.4	Kinematic distance	2.6	14	15.9 ± 1	7.7 ± 1.0
15	G8.7 – 0.1	4.5	Kinematic distance	36	7	4.5 ± 0.3	3.9 ± 0.3
16	G9.7 + 0.0	4.7	Kinematic distance	43	7	4.8 ± 0.2	3.7 ± 0.2
17	G9.9 – 0.8	4	Kinematic distance	31	14	3.8 ± 0.3	4.6 ± 0.3
18	G11.0 + 0.0	2.4 ± 0.7	Optical extinction	...	10	...	6 ± 0.7
19	G11.2 – 0.3	7.2	Kinematic distance	32	14	3.7 ± 0.2	4.8 ± 0.3
20	G12.0 – 0.1	10	Pulsar association	...	15	...	2.5
21	G12.2 + 0.3	11.8	Kinematic distance	50	14	11.6 ± 0.3	3.9 ± 0.3

Table 1 *continued*

Table 1 (*continued*)

#	SNR ^a	Literature	Method	V_{LSR} (km s ⁻¹)	Ref	Revised	Galactocentric
		dist (kpc)				dist ^b (kpc)	dist (kpc)
22	G12.8 + 0.0	4.7	Pulsar association	...	16	...	3.9
23	G13.3 - 1.3	3.3 ± 1.3	Kinematic distance	30**	17	3.1 ± 0.3	5.3 ± 0.3
24	G15.1 - 1.6	2.1	Optical extinction	...	10	...	6.3
25	G15.4 + 0.1	9.3 ± 1.3	Kinematic distance	95	18	9.8 ± 1.3	2.8 ± 0.8
26	G15.9 + 0.2	11.5 ± 4.5	Kinematic distance	...	19	...	4.2 ± 3.8
27	G16.0 - 0.5	3.4	CO observations	...	20	...	5.2
28	G16.7 + 0.1	14	Kinematic distance	20	19	13.9 ± 0.4	6.4 ± 0.4
29	G17.4 - 2.3	> 2.3	Estimation	...	21	...	> 8
30	G18.0 - 0.7 [†]	3.1 ± 0.2	Optical extinction	...	10	...	5.5 ± 0.2
31	G18.1 - 0.1	6.4 ± 0.2	Kinematic distance	103.74	22	...	3.0 ± 0.2
32	G18.6 - 0.2	4.4 ± 0.2	Kinematic distance	62.84	22	...	4.4 ± 0.2
33	G18.76 - 0.072 [†]	4.7 ± 0.3	Kinematic distance	70	23	...	4.2 ± 0.2
34	G18.8 + 0.3	13.8 ± 0.4	Kinematic distance	21.35	22	...	6.5 ± 0.4
35	G18.9 - 1.1	2.1 ± 0.4	Kinematic distance	23.27	24	...	6.4 ± 0.4
36	G20.0 - 0.2	11.2 ± 0.3	Kinematic distance	66.4	22	...	4.4 ± 0.2
37	G21.5 - 0.9	4.4 ± 0.2	Kinematic distance	67.79	22	...	4.5 ± 0.2
38	G21.8 - 3.0 [†]	0.33 ± 0.1	Kinematic distance	5.9	25	...	8.0 ± 0.2
39	G21.8 - 0.6	5.6 ± 0.2	Kinematic distance	93.35	22	...	3.8 ± 0.2
40	G22.7 - 0.2	4.7 ± 0.2	Kinematic distance	76.63	22	...	4.4 ± 0.2
41	G23.3 - 0.3	4.8 ± 0.2	Kinematic distance	78.51	22	...	4.4 ± 0.2
42	G24.7 - 0.6	3.8 ± 0.2	Kinematic distance	60.67	26	...	5.1 ± 0.2
43	G24.7 + 0.6	3.5 ± 0.2	Kinematic distance	54.6	27	...	5.4 ± 0.2
44	G25.1 - 2.3	2.9	Kinematic distance	39.2	28	2.7 ± 0.3	6 ± 0.3
45	G26.6 - 0.1 [‡]	1.3	Absorption column	...	29	...	7.2
46	G27.4 + 0.0	5.8 ± 0.3	Kinematic distance	99.95	22	...	4.2 ± 0.2
47	G28.6 - 0.1	9.6 ± 0.3	Kinematic distance	85	26	...	4.6 ± 0.1
48	G28.8 + 1.5	3.4 ± 0.6	Optical extinction	...	10	...	5.6 ± 0.4
49	G29.4 + 0.1 [‡]	6.5 ± 1	Kinematic distance	97	30	...	4.2 ± 0.2
50	G29.6 + 0.1	4.7 ± 0.3	Kinematic distance	80.16	27	...	4.8 ± 0.2
51	G29.7 - 0.3	5.6 ± 0.3	Kinematic distance	95	22	...	4.4 ± 0.2
52	G31.299 - 0.493 [†]	5 ± 0.3	Kinematic distance	85	23	...	4.8 ± 0.2
53	G31.9 + 0.0	7.1 ± 0.4	Kinematic distance	v_{TP}	31	...	4.4 ± 0.1
54	G32.1 - 0.9	2	Optical extinction	...	10	...	6.7
55	G32.4 + 0.1	11.8	Kinematic distance	43	14	11.3 ± 0.3	6.2 ± 0.2
56	G32.8 - 0.1	4.8 ± 0.3	Kinematic distance	81.81	22	...	5 ± 0.2
57	G33.6 + 0.1	3.5 ± 0.3	Kinematic distance	57.9	22	...	5.8 ± 0.2
58	G34.7 - 0.4	3 ± 0.3	Kinematic distance	50.48	22	...	6.1 ± 0.2
59	G35.6 - 0.4	3.8 ± 0.3	Kinematic distance	63.67	22	...	5.7 ± 0.2
60	G38.7 - 1.3	4	Absorption column	...	32	...	5.8
61	G39.2 - 0.3	8.5 ± 0.5	Kinematic distance	69.39	22	...	5.7 ± 0.2

Table 1 *continued*

Table 1 (*continued*)

#	SNR ^a	Literature	Method	V_{LSR} (km s ⁻¹)	Ref	Revised	Galactocentric
		dist (kpc)				dist ^b (kpc)	dist (kpc)
62	G39.7 - 2.0	4.9 ± 0.4	Kinematic distance	77	33	5.1 ± 0.4	5.5 ± 0.2
63	G40.5 - 0.5	3.4	Kinematic distance	55	34	3.4 ± 0.4	6.1 ± 0.2
64	G41.1 - 0.3	8.5 ± 0.5	Kinematic distance	...	22	...	5.9 ± 0.2
65	G41.5 + 0.4	4.1 ± 0.5	Kinematic distance	63.67	26	...	5.9 ± 0.2
66	G42.8 + 0.6	7.7	Pulsar association	...	35	...	5.9
67	G43.3 - 0.2	11.3 ± 0.4	Kinematic distance	12.55	22	...	7.8 ± 0.3
68	G43.9 + 1.6	3.1 ± 1.2	Kinematic distance	50	36	...	6.4 ± 0.5
69	G44.5 - 0.2 [‡]	4.1	Kinematic distance	60	37	4.1 ± 0.7	6.1 ± 0.3
70	G46.8 - 0.3	8.4 ± 3.6	Kinematic distance	$v_{TP} - 0$	22	...	6.6 ± 1.5
71	G49.2 - 0.7	5.4 ± 0.6	Kinematic distance	v_{TP}	22	...	6.3 ± 0.1
72	G51.04 + 0.07 [†]	7.7 ± 2.3	Kinematic distance	v_{TP}	38	7.2 ± 1.8	6.8 ± 0.5
73	G51.26 + 0.11 [†]	$v_{TP} - 37$...	6.6 ± 1.7	6.6 ± 0.4
74	G53.4 + 0.0	7.5	Sagittarius-Carina arm	...	39	...	7.2
75	G53.6 - 2.2	2.3 ± 0.8	Kinematic distance	27	40	7.8 ± 0.6	7.3 ± 0.2
76	G54.1 + 0.3	4.9 ± 0.8	Kinematic distance	53.66	22	...	6.8 ± 0.1
77	G54.4 - 0.3	6.6 ± 0.6	Kinematic distance	36.66	31	...	7 ± 0.2
78	G55.0 + 0.3	14	Kinematic distance	-46.2	41	13.1 ± 0.7	10.7 ± 0.5
79	G57.2 + 0.8	6.6 ± 0.7	Kinematic distance	...	42	...	7.3 ± 0.2
80	G59.5 + 0.1	2.3	Kinematic distance	28	43	2.7 ± 0.5	7.3 ± 0.2
81	G63.7 + 1.1	3.8 ± 1.5	Kinematic distance	18.7	44	...	7.5 ± 0.1
82	G64.5 + 0.9	11	Kinematic distance	-43	45	10.6 ± 0.7	10.3 ± 0.5
83	G65.1 + 0.6	9.3 ± 0.3	Kinematic distance	-23	45	8.8 ± 0.6	9.2 ± 0.4
84	G65.3 + 5.7	0.77 ± 0.2	Proper motion + v_{Exp}	...	46	...	8 ± 0.2
85	G65.7 + 1.2	1 ± 0.4	Kinematic distance	12	47	1.3 ± 0.4	7.9 ± 0.2
86	G65.8 - 0.5 [‡]	2.4 ^{+0.3} _{-0.5}	Optical extinction	...	10	...	7.7 ± 0.3
87	G66.0 + 0.0	2.3 ± 0.3	Optical extinction	...	10	...	7.7 ± 0.2
88	G67.6 + 0.9	2 ± 0.2	Optical extinction	...	10	...	7.8 ± 0.2
89	G67.7 + 1.8	2 ^{+3.7} _{-0.5}	Optical extinction	...	10	...	7.8 ^{+0.5} _{-0.2}
90	G69.0 + 2.7	1.5	Kinematic distance	12	48	1.6 ± 0.7	7.9 ± 0.2
91	G73.9 + 0.9	4.4 ± 0.1	Kinematic distance	2.1	49	4.2 ± 0.8	8.2 ± 0.2
92	G74.0 - 8.5	0.735 ± 0.025	Parallax measurement	...	50	...	8.2 ± 0.2
93	G74.9 + 1.2	6.1 ± 0.9	Optical extinction	...	51	...	9.0 ± 0.4
94	G75.2 + 0.1 [‡]	≥10	Absorption column	...	52	...	≥11.2
95	G76.9 + 1.0	8	PWN	...	53	...	10.2
96	G78.2 + 2.1	2.1 ± 0.4	Kinematic distance	-8	54	...	8.6 ± 0.2
97	G82.2 + 5.3	3.2 ± 0.4	Optical extinction	...	10	...	8.5 ± 0.2
98	G84.2 - 0.8	6 ± 0.2	Kinematic distance	-48	55	7 ± 0.7	10.3 ± 0.4
99	G85.4 + 0.7	4.4 ± 0.8	Optical extinction	...	10	...	9.1 ± 0.4
100	G85.9 - 0.6	4.8 ± 1.6	Kinematic distance	32	56	...	9.3 ± 0.7
101	G89.0 + 4.7	1.9 ^{+0.3} _{-0.2}	Optical extinction	...	10	...	8.5 ± 0.2

Table 1 *continued*

Table 1 (*continued*)

#	SNR ^a	Literature	Method	<i>V</i> _{LSR}	Ref	Revised	Galactocentric
		dist (kpc)		(km s ⁻¹)		dist ^b (kpc)	dist (kpc)
102	G93.3 + 6.9	2.2 ± 0.5	HI column density	...	57	...	8.7 ± 0.2
103	G93.7 - 0.2	1.5 ± 0.2	Kinematic distance	-6	58	1.3 ± 0.2	8.5 ± 0.2
104	G94.0 + 1.0	3	Kinematic distance	-13	59	2.2 ± 0.8	8.8 ± 0.3
105	G96.0 + 2.0	4	Kinematic distance	-44	60	4.9 ± 0.7	10.1 ± 0.4
106	G106.3 + 2.7	0.8	Kinematic distance	-6.4	61	0.7 ± 0.5	8.5 ± 0.2
107	G107.0 + 9.0 [†]	1.75 ± 0.25	Kinematic distance	...	62	...	9 ± 0.2
108	G107.5 - 1.5 [‡]	1.1	Kinematic distance	-9	63	0.9	8.6
109	G108.2 - 0.6	3.2 ± 0.6	Kinematic distance	-55	64	...	9.8 ± 0.4
110	G109.1 - 1.0	3.1 ± 0.2	Kinematic distance	-50 ± 6	65	...	9.8 ± 0.2
111	G111.7 - 2.1	3.33 ± 0.1	Proper motion	-40**	66	3.3 ± 0.6	10 ± 0.4
112	G113.0 + 0.2	3.1	Kinematic distance	-50	60	3.2 ± 0.7	10 ± 0.5
113	G114.3 + 0.3	0.7	Kinematic distance	-6.5	67	0.5 ± 0.4	8.5 ± 0.2
114	G116.5 + 1.1	1.6	Kinematic distance	-17	67	1.3 ± 0.6	9 ± 0.4
115	G116.9 + 0.2	1.6	Kinematic distance	-27	67	2.1 ± 0.6	9.4 ± 0.4
116	G119.5 + 10.2	1.4 ± 0.3	Kinematic distance	-16	68	1.2 ± 0.2	9.0 ± 0.2
117	G120.1 + 1.4	4 ± 1	Proper motion + <i>v</i> _{Exp}	...	69	...	10.9 ± 0.8
118	G126.2 + 1.6	5.6 ± 0.3	Kinematic distance	-39--45	70	3.2 ± 0.6	10.5 ± 0.5
119	G127.1 + 0.5	1.15	Kinematic distance	-14	71	0.96 ± 0.5	8.9 ± 0.4
120	G130.7 + 3.1	2 ± 0.3	Perseus arm	...	72	...	9.8 ± 0.3
121	G132.7 + 1.3	1.95 ± 0.04	Kinematic distance	-45	73	...	9.8 ± 0.2
122	G141.2 + 5.0 [‡]	4 ± 0.5	Kinematic distance	53	74	...	11.7 ± 0.5
123	G150.3 + 4.5	0.7-4.5	Sedov estimates	...	75	...	10.7 ± 1.8
124	G152.4 - 2.1	1.1 ± 0.1	Kinematic distance	12	76	1.1 ± 0.4	9.3 ± 0.4
125	G156.2 + 5.7	≥1.7/ 1-3	Proper motion + <i>v</i> _{Shock}	...	77
126	G159.6 + 7.3	1-2.5	Diameter estimation	...	78	...	10 ± 0.7
127	G160.9 + 2.6	0.8 ± 0.4	Kinematic distance	-6	79	0.7 ± 0.4	9 ± 0.4
128	G166.0 + 4.3	1 ± 0.4	Kinematic distance	-6	80	...	9.3 ± 0.4
129	G172.8 + 1.5 [‡]	1.8	HII distance	-20	81	...	10.1
130	G179.0 + 2.6	< 5	Estimation	...	82	...	8.34 < R < 13.3
131	G180.0 - 1.7	1.333 ^{+0.103} _{-0.112}	Kinematic distance	...	83	...	9.7 ± 0.2
132	G181.1 + 9.5	1.5 ± 1	High V HI clouds	...	84	...	9.8 ± 1.0
133	G184.6 - 5.8	3.37 ^{+4.04} _{-0.97}	Parallax measurement	...	85	...	11.7 ^{+4.04} _{-0.98}
134	G189.1 + 3.0	1.729 ^{+0.116} _{-0.094}	MC association	...	86	...	10.1 ± 0.2
135	G189.6 + 3.3 [‡]	1.5 ± 0.2	Object associations	...	87	...	9.8 ± 0.3
136	G190.9 - 2.2	1.036 ^{+0.079} _{-0.087}	MC association	...	86	...	9.4 ± 0.2
137	G205.5 + 0.5	1.15 ± 0.3	MC association	...	86	...	9.4 ± 0.3
138	G206.9 + 2.3	2.2	Kinematic distance	22 ± 5	88	2.2 ± 0.7	10.3 ± 0.7
139	G213.0 - 0.6	1.146 ^{+0.079} _{-0.080}	MC association	...	86	...	9.4 ± 0.2
140	G260.4 - 3.4	1.3 ± 0.3	Kinematic distance	10	89	1.4 ± 0.8	8.7 ± 0.3
141	G263.9 - 3.3	0.25 ± 0.03	Parallax measurement	...	90	...	8.4 ± 0.2

Table 1 *continued*

Table 1 (*continued*)

#	SNR ^a	Literature	Method	V_{LSR} (km s ⁻¹)	Ref	Revised	Galactocentric
		dist (kpc)				dist ^b (kpc)	dist (kpc)
142	G266.2 – 1.2	0.7 ± 0.2	MC association	...	91	...	8.4 ± 0.2
143	G267.0 – 1.0 [‡]	≤0.9	MC association	...	92	...	8.39 ± 0.05
144	G272.2 – 3.2	2–10	Stats + optical color excess	...	93	...	10.1 ± 2.3
145	G276.5 + 19.0 [‡]	0.2 ± 0.14	²⁶ Al γ-ray emission	...	94	...	8.3 ± 0.2
146	G279.0 + 1.1	2.7 ± 0.3	Optical extinction	...	95	...	8.4 ± 0.2
147	G284.3 – 1.8	5.5 ± 0.7	Optical extinction	...	95	...	8.8 ± 0.3
148	G290.1 – 0.8	7 ± 1	Kinematic distance	7	96	6.3 ± 0.8	8.9 ± 0.5
149	G291.0 – 0.1	3.5	HII distance	...	97	...	7.8
150	G292.0 + 1.8	6.2 ± 0.9	Kinematic distance	0	98	6.2 ± 0.8	8.6 ± 0.3
151	G292.2 – 0.5	8.4 ± 0.4	Kinematic distance	22	99	8.1 ± 0.6	9.2 ± 0.3
152	G296.1 – 0.5	4.3 ± 0.8	Optical extinction	...	95	...	7.5 ± 0.2
153	G296.5 + 10.0	2.1 ^{+1.8} _{-0.8}	Kinematic distance	-16	100	...	7.6 ^{+0.4} _{-0.2}
154	G296.7 – 0.9	9.8 ^{+1.1} _{-0.7}	Sedov estimates	...	101	...	9.7 ± 0.6
155	G296.8 – 0.3	9.6 ± 0.6	Kinematic distance	23	102	9.3 ± 0.6	9.3 ± 0.4
156	G298.6 + 0.0	10	Absorption column	...	103	...	9.5
157	G299.2 – 2.9	2.8 ± 0.8	Optical extinction	...	95	...	7.4 ± 0.2
158	G304.6 + 0.1	9.7	Kinematic distance	-20	104	7.9 ± 0.6	7.5 ± 0.3
159	G306.3 – 0.9	20	Absorption column	...	105	...	16.5
160	G308.4 – 1.4	5 ± 0.7	Optical extinction	...	95	...	6.5 ± 0.1
161	G308.8 – 0.1	5.4	Estimation	...	106	...	6.5
162	G309.2 – 0.6	2.8 ± 0.8	Optical extinction	...	95	...	6.9 ± 0.3
163	G309.8 – 2.6 [‡]	2.3 ± 0.2	Optical extinction	...	95	...	7.1 ± 0.2
164	G310.6 – 1.6	7	Crux–Scutum arm	...	107	...	6.5
165	G311.5 – 0.3	> 6.6	Kinematic distance	-10	104	10.3 ± 0.5	7.9 ± 0.3
166	G312.4 – 0.4	> 6	Kinematic distance	-50	108	3.5 ± 0.5	6.5 ± 0.2
167	G313.3 + 0.1 [‡]	5.6	PWN	...	53	...	6.1
168	G315.1 + 2.7	1.7	Estimation	...	109	...	7.2
169	G315.4 – 2.3	2.8 ± 0.4	Kinematic distance	-33.2	110	2.2 ± 0.4	6.9 ± 0.3
170	G316.3 + 0.0	> 7.2	Kinematic distance	-40	104	9.4 ± 0.4	6.7 ± 0.2
171	G318.2 + 0.1	3.5 ± 0.2	Kinematic distance	-42	111	2.7 ± 0.4	6.6 ± 0.3
172	G320.4 – 1.2	5.2 ± 1.4	Kinematic distance	-55–70	112	...	5.5 ± 0.3
173	G322.1 + 0.0	9.4 ^{+0.8} ₋₁	Kinematic distance	...	113	...	5.8 ^{+0.4} _{-0.5}
174	G323.7 – 1.0	3.5	Scutum-Crux arm	...	114	...	5.9
175	G326.3 – 1.8	4.1 ± 0.7	Kinematic distance	-58	110	3.5 ± 0.6	5.8 ± 0.4
176	G327.1 – 1.1	9	Absorption column	...	115	...	5
177	G327.2 – 0.1	4.5 ± 0.5	CO observations	...	116	...	5.2 ± 0.3
178	G327.4 + 0.4	4.3 ± 0.5	Kinematic distance	-75	117	4.4 ± 0.5	5.2 ± 0.3
179	G327.6 + 14.6	2.18 ± 0.08	Proper motion + v_{Shock}	...	118	...	6.6 ± 0.2
180	G328.4 + 0.2	> 17.4 ± 0.9	Kinematic distance	28	119	> 16.7 ± 0.7	> 10.5 ± 0.6
181	G330.0 + 15.0	1.2	Estimation	...	120	...	7.3

Table 1 *continued*

Table 1 (*continued*)

#	SNR ^a	Literature	Method	V_{LSR}	Ref	Revised	Galactocentric
		dist (kpc)		(km s ⁻¹)		dist ^b (kpc)	dist (kpc)
182	G330.2 + 1.0	> 4.9 ± 0.3	Kinematic distance	...	117	...	> 4.1 ± 0.2
183	G332.4 – 0.4	3.0 ± 0.3	Optical extinction	...	95	...	5.8 ± 0.3
184	G332.4 + 0.1	9.2 ± 1.7	Norma arm	...	121	...	4.3 ± 0.7
185	G332.5 – 5.6	3 ± 0.8	Optical extinction	...	122	...	5.8 ± 0.6
186	G335.2 + 0.1	1.8 ± 0.4	Kinematic distance	-22.5	123	1.7 ± 0.4	6.8 ± 0.4
187	G337.0 – 0.1	11 ± 0.3	Kinematic distance	-72	124	10.8 ± 0.3	4.5 ± 0.2
188	G337.2 – 0.7	5.5 ± 4	Kinematic distance	-100	125	9.4 ± 0.3	3.7 ± 0.1
189	G337.2 + 0.1	14	Kinematic distance	...	126	...	7.1
190	G337.8 – 0.1	12.3	Kinematic distance	-45	127	12.2 ± 0.3	5.5 ± 0.3
191	G338.3 + 0.0	8.5-13	Kinematic distance	-31	128	13 ± 0.4	6.1 ± 0.4
192	G338.5 + 0.1	11	Norma arm	...	129	...	4.5
193	G340.6 + 0.3	15	Scutum-Crux arm	...	129	...	7.7
194	G341.2 + 0.9	6.9	Pulsar association	...	130	...	2.9
195	G341.9 – 0.3	0	127	15.8 ± 0.6	8.3 ± 0.6
196	G342.0 – 0.2	0	127	15.8 ± 0.6	8.3 ± 0.6
197	G343.0 – 6.0	1.2 ± 0.2	Civ luminosity estimation	...	131, 132	...	7.4 ± 0.2
198	G343.1 – 0.7	-70	127	4.9 ± 0.2	3.9 ± 0.2
199	G344.7 – 0.1	6.3 ± 0.1	Kinematic distance	-115	133	...	2.8 ± 0.1
200	G346.6 – 0.2	5.5/11	Kinematic distance	-76	127	10.4 ± 0.2	3.0 ± 0.2
201	G347.3 – 0.5	1	Kinematic distance	-6	134	0.9 ± 0.6	7.5 ± 0.6
202	G348.5 + 0.0	≤ 6.3	Kinematic distance	-100**	135	7.2 ± 0.2	1.9 ± 0.1
203	G348.5 + 0.1	6.3 - 9.5	Kinematic distance	-107--145	135	...	1.7 ± 0.3
204	G348.7 + 0.3	13.2 ± 0.2	Kinematic distance	26	135	...	5.3 ± 0.2
205	G349.7 + 0.2	11.5 ± 0.7	3 kpc arm	...	136	...	3.6 ± 0.7
206	G350.0 – 2.0	3	Optical extinction	...	137	...	5.4
207	G350.1 – 0.3	9 ± 3	Absorption column	...	138	...	1.6 ± 1.4
208	G351.7 + 0.8	13.2 ± 0.5	Kinematic distance	-14	139	14 ± 0.6	5.9 ± 0.6
209	G352.7 – 0.1	7.5 ± 0.5	Kinematic distance	...	140	...	1.3 ± 0.3
210	G353.6 – 0.7	3.2 ± 0.8	Kinematic distance	-30	141	4.8 ± 0.8	3.6 ± 0.8
211	G354.4 + 0.0 [‡]	5 - 8	Kinematic distance	...	142	...	2 ± 0.2
212	G354.8 – 0.8	-70	127	8.3 ± 0.2	1
213	G355.6 + 0.0	13	Absorption column	...	143	...	4.7
214	G357.7 – 0.1	11.8	Kinematic distance	-12.4	144	11.5 ± 0.7	3.2 ± 0.7
215	G359.1 – 0.5	5	Kinematic distance	...	145	...	3.3

Table 1 *continued*

Table 1 (*continued*)

#	SNR ^a	Literature	Method	V_{LSR}	Ref	Revised	Galactocentric
				(km s ⁻¹)		dist ^b (kpc)	dist (kpc)

NOTE—a - † indicates new SNRs that are not in the catalogue presented by Green (2019) and ‡ indicates uncertain SNRs (I.e. more observational evidence is needed).

b - The distances for most SNRs and the errors are recalculated using the rotaion curve parameters presented by Reid et al. (2014).

*- The V_{LSR} is from Hewitt & Yusef-Zadeh (2009)

**- The V_{LSR} is from Koralesky et al. (1998)

References : (1) Reid (1993), (2) Kassim & Frail (1996), (3) Aharonian et al. (2005), (4) Pihlström et al. (2014), (5) Reynolds et al. (2008), (6) Sankrit et al. (2016), (7) Hewitt & Yusef-Zadeh (2009), (8) Frail et al. (1994b), (9) Liszt (2009), (10) Shan et al. (2018), (11) Velázquez et al. (2002), (12) Roberts & Brogan (2008), (13) Milne et al. (1986), (14) Kilpatrick et al. (2016), (15) Yamauchi et al. (2014), (16) Gotthelf & Halpern (2009), (17) Seward et al. (1995), (18) Su et al. (2017a), Tian et al. (2019), (20) Beaumont et al. (2011), (21) Boumis et al. (2002), (22) Ranasinghe & Leahy (2018b), (23) Ranasinghe et al. (2021), (24) Ranasinghe et al. (2020), (25) Gao et al. (2020) , (26) Ranasinghe & Leahy (2018a), (27) Ranasinghe et al. (2018), (28) Gao et al. (2011), (29) Bamba et al. (2003) , (30) Petriella (2019), (31) Ranasinghe & Leahy (2017), (32) Huang et al. (2014), (33) Su et al. (2018), (34) Yang et al. (2006), (35) Lorimer & Xilouris (2000) (36) Zhou et al. (2020b), (37) Su et al. (2017b), (38) Supan et al. (2018), (39) Driessen et al. (2018), (40) Giacani et al. (1998), (41) Matthews et al. (1998), (42) Zhou et al. (2020a), (43) Xu & Wang (2012), (44) Wallace et al. (1997), (45) Tian & Leahy (2006a), (46) Boumis et al. (2004), (47) Kothes et al. (2008), (48) Leahy & Ranasinghe (2012), (49) Zdziarski et al. (2016), (50) Fesen et al. (2018), (51) Kothes et al. (2003), (52) Hessels et al. (2004), (53) Kargaltsev & Pavlov (2010), (54) Leahy et al. (2013) , (55) Leahy & Green (2012), (56) Jackson et al. (2008), (57) Foster & Routledge (2003) , (58) Uyaniker et al. (2002), (59) Jeong et al. (2013), (60) Kothes et al. (2005), (61) Kothes et al. (2001), (62) Fesen et al. (2020), (63) Kothes (2003), (64) Tian et al. (2007b), (65) Sánchez-Cruces et al. (2018), (66) Alarie et al. (2014), (67) Yar-Uyaniker et al. (2004), (68) Pineault et al. (1993), (69) Hayato et al. (2010), (70) Tian & Leahy (2006b), (71) Leahy & Tian (2006), (72) Kothes (2013), (73) Zhou et al. (2016), (74) Kothes et al. (2014), (75) Devin et al. (2020), (76) Foster et al. (2013), (77) Katsuda et al. (2016), (78) Fesen & Milisavljevic (2010), (79) Leahy & Tian (2007), (80) Arias et al. (2019), (81) Kang et al. (2012), (82) How et al. (2018), (83) Dinçel et al. (2015), (84) Kothes et al. (2017), (85) Fraser & Boubert (2019), (86) Yu et al. (2019), (87) Asaoka & Aschenbach (1994), (88) Ambrocio-Cruz et al. (2014), (89) Reynoso et al. (2017), (90) Cha et al. (1999), (91) Allen et al. (2015), (92) Acero et al. (2013), (93) Sezer & Gök (2012), (94) McCullough et al. (2002), (95) Shan et al. (2019), (96) Reynoso et al. (2006), (97) Roger et al. (1986), (98) Gaensler & Wallace (2003), (99) Caswell et al. (2004), (100) Giacani et al. (2000), (101) Prinz & Becker (2013), (102) Gaensler et al. (1998), (103) Bamba et al. (2016), (104) Caswell et al. (1975), (105) Sawada et al. (2019), (106) Wilson (1986), (107) Renaud et al. (2010), (108) Doherty et al. (2003), (109) Stupar et al. (2007), (110) Rosado et al. (1996), (111) Hofverberg et al. (2010), (112) Gaensler et al. (1999), (113) Heinz et al. (2015), (114) Maxted et al. (2018), (115) Sun et al. (1999), (116) Tiengo et al. (2010), (117) McClure-Griffiths et al. (2001), (118) Winkler et al. (2003), (119) Gaensler et al. (2000), (120) Leahy et al. (1991), (121) Vink (2004), (122) Zhu et al. (2015), (123) Eger et al. (2011), (124) Sarma et al. (1997), (125) Rakowski et al. (2006), (126) Combi et al. (2005), (127) Koralesky et al. (1998), (128) Supan et al. (2016), (129) Kothes & Dougherty (2007), (130) Frail et al. (1994a), (131) Welsh et al. (2003), (132) Kim et al. (2010), (133) Giacani et al. (2011), (134) Fukui et al. (2003), (135) Tian & Leahy (2012), (136) Tian & Leahy (2014), (137) Karpova et al. (2016), (138) Yasumi et al. (2014), (139) Tian et al. (2007a), (140) Giacani et al. (2009), (141) Tian et al. (2008), (142) Roy & Pal (2013), (143) Minami et al. (2013), (144) Frail et al. (1996), (145) Frail (2011).

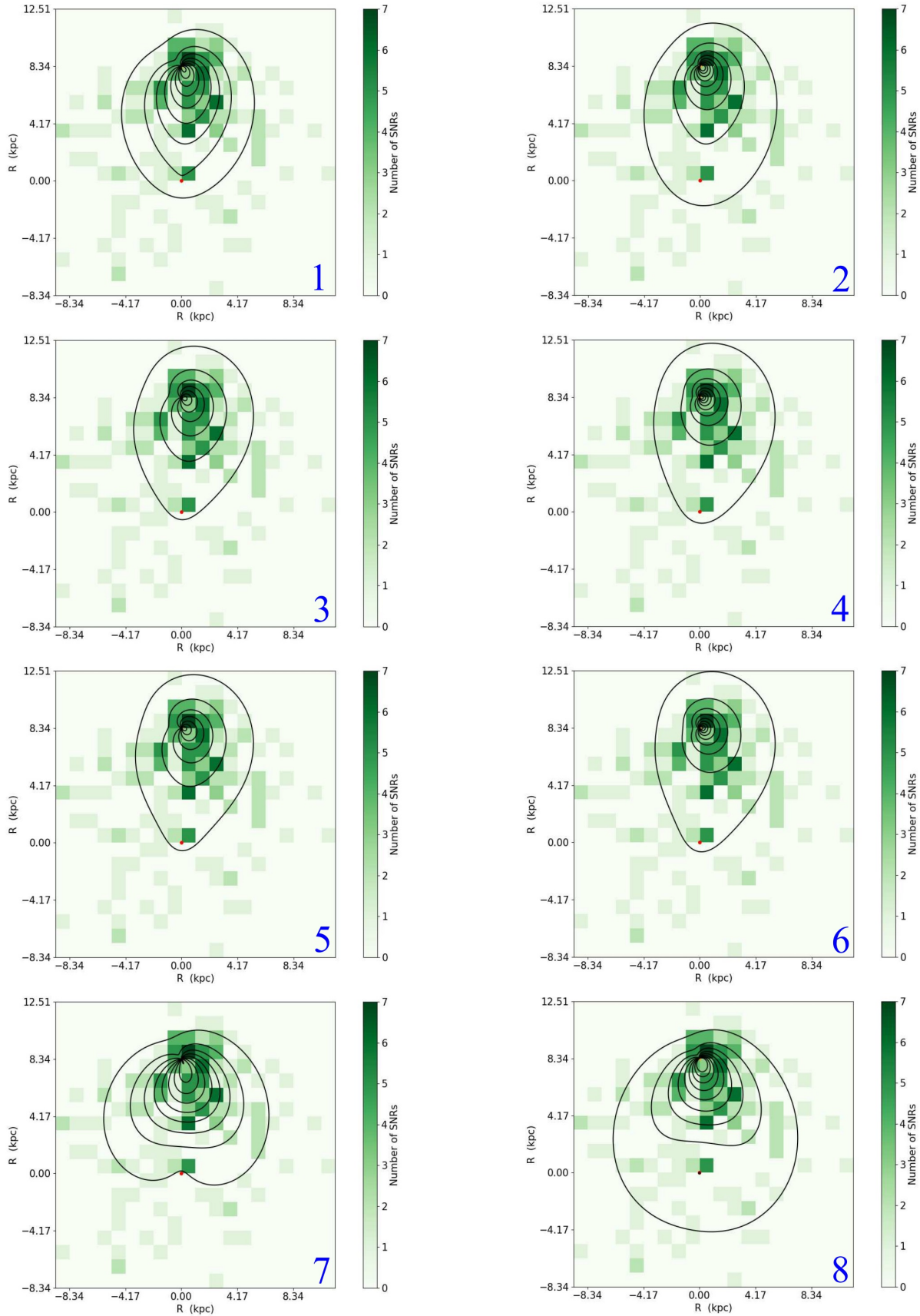
Table 3. SNR Surface Density and Correction Factor Model Parameters from Method 2

#	Models	Parameters	Y^2	# of SNRs ^a
1	Exp - Exp	$A = 71.0 \pm 20.0 \text{ kpc}^{-2}$, $H_R = 3.41_{-0.45}^{+0.42} \text{ kpc}$, $H_S = 1.95_{-0.33}^{+0.30} \text{ kpc}$, $B = 0.60_{-0.19}^{+0.24}$, $l_0 = 131^\circ_{-27^\circ}{}^{+33^\circ}$	166.76	4950_{-2210}^{+2840}
2	Exp - PLC	$A = 42.2 \pm 12.9 \text{ kpc}^{-2}$, $H_R = 4.99_{-0.97}^{+1.03} \text{ kpc}$, $R_S = 3.60_{-0.78}^{+0.74} \text{ kpc}$, $\alpha_2 = 3.18_{-0.38}^{+0.57}$, $B = 0.49_{-0.23}^{+0.33}$, $l_0 = 116^\circ_{-42^\circ}{}^{+49^\circ}$	165.06	5590_{-2730}^{+3990}
3	PLC ^b - Exp	$A = 45.0 \pm 13.1 \text{ kpc}^{-2}$, $R_c = 4.29_{-1.00}^{+1.02} \text{ kpc}$, $\alpha_1 = 2$, $H_S = 2.06_{-0.37}^{+0.34} \text{ kpc}$, $B = 0.52_{-0.26}^{+0.38}$, $l_0 = 98^\circ_{-41^\circ}{}^{+43^\circ}$	168.31	4120_{-2020}^{+2700}
4	PLC ^b - PLC	$A = 31.2 \pm 9.6 \text{ kpc}^{-2}$, $R_c = 7.83_{-2.35}^{+2.75} \text{ kpc}$, $\alpha_1 = 2$, $R_S = 3.47_{-0.77}^{+0.74} \text{ kpc}$, $\alpha_2 = 3.04_{-0.37}^{+0.56}$, $B = 0.46_{-0.27}^{+0.44}$, $l_0 = 90^\circ_{-53^\circ}{}^{+54^\circ}$	166.31	5530_{-2910}^{+4060}
5	PLC ^c - Exp	$A = 52.1 \pm 16.2 \text{ kpc}^{-2}$, $R_c = 2.26_{-0.62}^{+0.64} \text{ kpc}$, $\alpha_1 = 1.5$, $H_S = 2.06_{-0.40}^{+0.36} \text{ kpc}$, $B = 0.52_{-0.28}^{+0.44}$, $l_0 = 93^\circ_{-45^\circ}{}^{+47^\circ}$	168.37	4150_{-2150}^{+2940}
6	PLC ^c - PLC	$A = 30.0 \pm 9.3 \text{ kpc}^{-2}$, $R_c = 5.21_{-1.72}^{+2.06} \text{ kpc}$, $\alpha_1 = 1.5$, $R_S = 3.52_{-0.79}^{+0.75} \text{ kpc}$, $\alpha_2 = 3.05_{-0.37}^{+0.56}$, $B = 0.46_{-0.28}^{+0.46}$, $l_0 = 85^\circ \pm 54^\circ$	166.57	5510_{-2900}^{+4040}
7	GD - Exp	$A = 14.0 \pm 4.2 \text{ kpc}^{-2}$, $\mu = 3.66_{-0.95}^{+0.78} \text{ kpc}$, $\sigma = 3.37 \pm 0.55 \text{ kpc}$, $H_S = 2.54_{-0.56}^{+0.55} \text{ kpc}$, $B = 0.62 \pm 0.26$, $l_0 = 145^\circ_{-28^\circ}{}^{+32^\circ}$	163.95	2900_{-1610}^{+2370}
8	GD - PLC	$A = 19.3 \pm 6.2 \text{ kpc}^{-2}$, $\mu = 4.10_{-1.08}^{+0.89} \text{ kpc}$, $\sigma = 3.32_{-0.66}^{+0.69} \text{ kpc}$, $R_S = 2.46 \pm 0.66 \text{ kpc}$, $\alpha_2 = 2.22_{-0.30}^{+0.46}$, $B = 0.57 \pm 0.30$, $l_0 = 144^\circ_{-33^\circ}{}^{+38^\circ}$	161.07	4310_{-2550}^{+4000}
9	$GD_{\mu=0}$ - Exp	$A = 32.2 \pm 8.9 \text{ kpc}^{-2}$, $\sigma = 4.56_{-0.43}^{+0.40} \text{ kpc}$, $H_S = 2.19_{-0.40}^{+0.37} \text{ kpc}$, $B = 0.66 \pm 0.22$, $l_0 = 145^\circ_{-22^\circ}{}^{+27^\circ}$	164.58	4200_{-1700}^{+2110}
10	$GD_{\mu=0}$ - PLC	$A = 32.4 \pm 9.7 \text{ kpc}^{-2}$, $\sigma = 5.10_{-0.63}^{+0.61} \text{ kpc}$, $R_S = 3.20_{-0.72}^{+0.69} \text{ kpc}$, $\alpha_2 = 2.82_{-0.34}^{+0.51}$, $B = 0.57 \pm 0.29$, $l_0 = 139^\circ_{-31^\circ}{}^{+37^\circ}$	162.44	5270_{-2410}^{+3230}
11	MGF - Exp	$A = 5.7 \pm 1.7 \text{ kpc}^{-2}$, $\alpha_1 = 3.71_{-0.71}^{+1.26} \text{ kpc}$, $\beta = 7.50_{-1.43}^{+0.98}$, $H_S = 2.38_{-0.52}^{+0.51} \text{ kpc}$, $B = 0.68_{-0.16}^{+0.20}$, $l_0 = 148^\circ_{-25^\circ}{}^{+28^\circ}$	165.04	3320_{-1640}^{+5210}
12	MGF - PLC	$A = 8.9 \pm 2.9 \text{ kpc}^{-2}$, $\alpha_1 = 3.70_{-0.71}^{+1.33} \text{ kpc}$, $\beta = 7.10_{-1.51}^{+0.99}$, $R_S = 2.32_{-0.62}^{+0.61} \text{ kpc}$, $\alpha_2 = 2.23_{-0.30}^{+0.46}$, $B = 0.60_{-0.18}^{+0.24}$, $l_0 = 146^\circ_{-31^\circ}{}^{+36^\circ}$	162.15	4790_{-2010}^{+6910}
13	CB98e15 - Exp	$A = 17.7 \pm 5.8 \text{ kpc}^{-2}$, $R_a = 15.70_{-1.78}^{+2.62} \text{ kpc}$, $\theta_0 = 0.69_{-0.29}^{+0.25}$, $\beta = 0.11_{-0.04}^{+0.05}$, $H_S = 2.56_{-0.61}^{+0.59} \text{ kpc}$, $B = 0.57_{-0.21}^{+0.28}$, $l_0 = 135^\circ_{-35^\circ}{}^{+40^\circ}$	163.69	2570_{-1630}^{+3960} *
14	CB98e15 - PLC	$A = 28.8 \pm 9.9 \text{ kpc}^{-2}$, $R_a = 14.02_{-1.87}^{+3.33} \text{ kpc}$, $\theta_0 = 0.35_{-0.42}^{+0.33}$, $\beta = 0.13_{-0.04}^{+0.06}$, $R_S = 2.77 \pm 0.78 \text{ kpc}$, $\alpha_2 = 2.36_{-0.34}^{+0.55}$, $B = 0.52_{-0.22}^{+0.30}$, $l_0 = 136^\circ_{-41^\circ}{}^{+47^\circ}$	161.16	3810_{-2470}^{+6310} *
15	Sérsic - Exp	$A = 8.3 \pm 2.5 \text{ kpc}^{-2}$, $R_e = 6.24_{-0.65}^{+0.62} \text{ kpc}$, $n = 0.25_{-0.16}^{+0.52}$, $b_n = 0.23$ $(^{1.22}_{0.02})^d$, $H_S = 2.72 \pm 0.61 \text{ kpc}$, $B = 0.56 \pm 0.30$, $l_0 = 138^\circ_{-33^\circ}{}^{+37^\circ}$	163.42	2380_{-1210}^{+2780}
16	Sérsic - PLC	$A = 13.0 \pm 4.1 \text{ kpc}^{-2}$, $R_e = 6.3 \pm 0.7 \text{ kpc}$, $n = 0.25_{-0.17}^{+0.50}$, $b_n = 0.23$ $(^{1.20}_{0.01})^d$, $R_S = 2.80 \pm 0.75 \text{ kpc}$, $\alpha_2 = 2.32_{-0.32}^{+0.50}$, $B = 0.54 \pm 0.32$, $l_0 = 140^\circ_{-37^\circ}{}^{+42^\circ}$	160.94	3790_{-2050}^{+4680}

NOTE—a - The total number of SNRs estimated to galactocentric distance, $R = 16.68 \text{ kpc}$. b,c - SNR surface density, $\rho_{SNR}(R)$ follows a power-law distribution where α_1 is set to 2 and 1.5, respectively.

* - The total number of SNRs are calculated up to a $R < R_a(1 - \theta_0/\pi)$

d - b_n values calculated by using the lower and upper limits of n



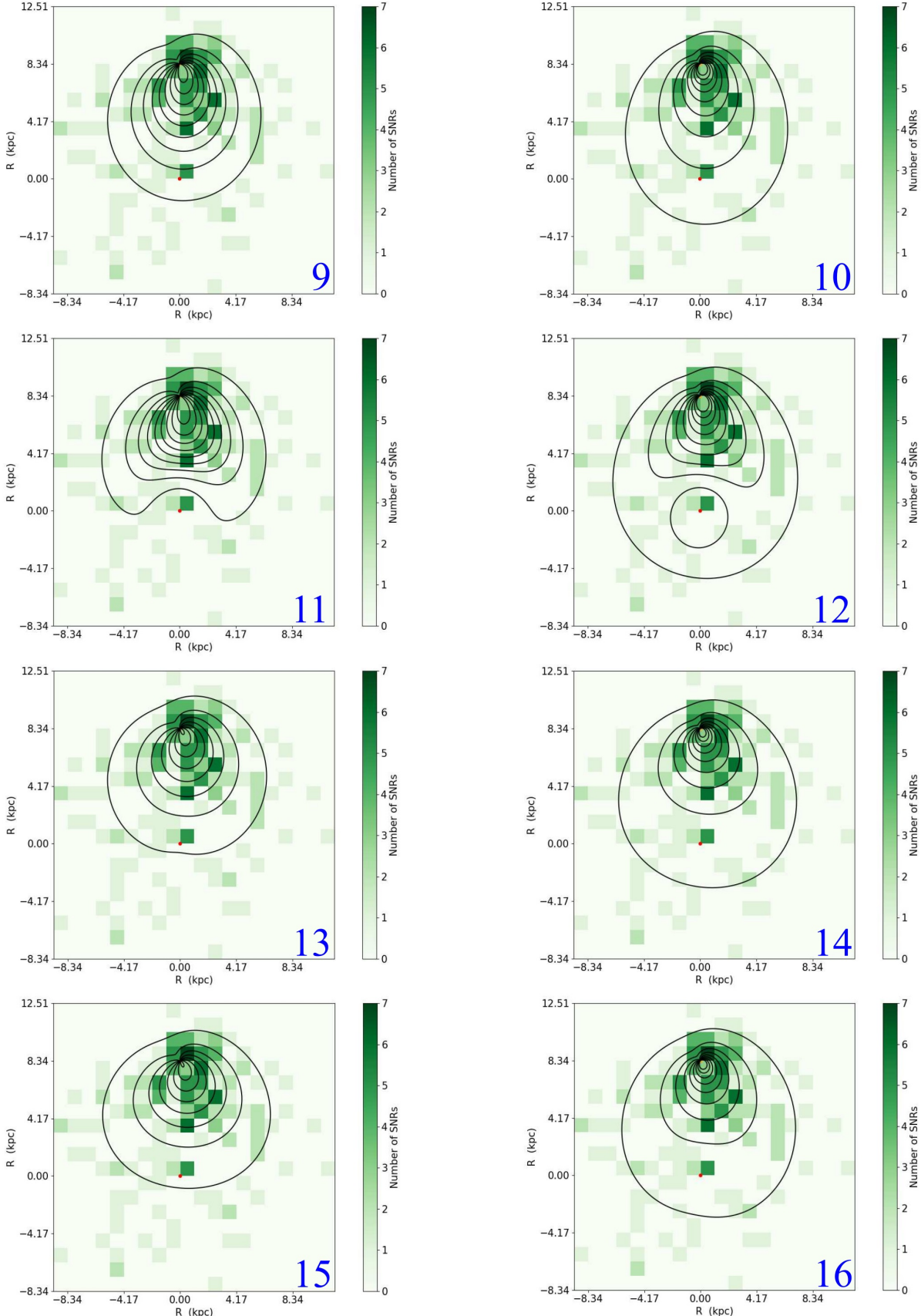


Figure 8. The model distributions from Method 2 (product of the SNR surface density functions and selection functions: $A\rho_{SNR}(R)f_{sel}(d,l)$) with black contours at $0.5, 1.5, 2.5, \dots$ kpc^{-2} . The numbers in each panel corresponds to the model numbers in Table 3. The 1.0425×1.0425 kpc green squares represents the observed number of SNR contained in each area according to the color bars at the left of each panel. The red circle indicates GC and the yellow circle the Sun. The panel numbers correspond to the model numbers given in Table 3.

REFERENCES

- Acero, F., Gallant, Y., Ballet, J., Renaud, M., & Terrier, R. 2013, A&A, 551, A7, doi: [10.1051/0004-6361/201220799](https://doi.org/10.1051/0004-6361/201220799)
- Aharonian, F., Akhperjanian, A. G., Aye, K. M., et al. 2005, A&A, 432, L25, doi: [10.1051/0004-6361:200500022](https://doi.org/10.1051/0004-6361:200500022)
- Alarie, A., Bilodeau, A., & Drissen, L. 2014, MNRAS, 441, 2996, doi: [10.1093/mnras/stu774](https://doi.org/10.1093/mnras/stu774)
- Allen, G. E., Chow, K., DeLaney, T., et al. 2015, ApJ, 798, 82, doi: [10.1088/0004-637X/798/2/82](https://doi.org/10.1088/0004-637X/798/2/82)
- Ambrocio-Cruz, P., Rosado, M., Le Coarer, E., Bernal, A., & Gutiérrez, L. 2014, RMxAA, 50, 323
- Anderson, L. D., & Bania, T. M. 2009, ApJ, 690, 706, doi: [10.1088/0004-637X/690/1/706](https://doi.org/10.1088/0004-637X/690/1/706)
- Anderson, L. D., Bania, T. M., Balser, D. S., & Rood, R. T. 2012, ApJ, 754, 62, doi: [10.1088/0004-637X/754/1/62](https://doi.org/10.1088/0004-637X/754/1/62)
- Anderson, L. D., Wang, Y., Bihr, S., et al. 2017, A&A, 605, A58, doi: [10.1051/0004-6361/201731019](https://doi.org/10.1051/0004-6361/201731019)
- Arias, M., Domček, V., Zhou, P., & Vink, J. 2019, A&A, 627, A75, doi: [10.1051/0004-6361/201935528](https://doi.org/10.1051/0004-6361/201935528)
- Asaoka, I., & Aschenbach, B. 1994, A&A, 284, 573
- Auchettl, K., Ng, C. Y., Wong, B. T. T., Lopez, L., & Slane, P. 2017, ApJ, 847, 121, doi: [10.3847/1538-4357/aa830e](https://doi.org/10.3847/1538-4357/aa830e)
- Bamba, A., Sawada, M., Nakano, Y., et al. 2016, PASJ, 68, S5, doi: [10.1093/pasj/psv096](https://doi.org/10.1093/pasj/psv096)
- Bamba, A., Ueno, M., Koyama, K., & Yamauchi, S. 2003, ApJ, 589, 253, doi: [10.1086/374354](https://doi.org/10.1086/374354)
- Beaumont, C. N., Williams, J. P., & Goodman, A. A. 2011, ApJ, 741, 14, doi: [10.1088/0004-637X/741/1/14](https://doi.org/10.1088/0004-637X/741/1/14)
- Becker, R. H., Markert, T., & Donahue, M. 1985, ApJ, 296, 461, doi: [10.1086/163465](https://doi.org/10.1086/163465)
- Beuther, H., Bihr, S., Rugel, M., et al. 2016, A&A, 595
- Bland-Hawthorn, J., & Gerhard, O. 2016, ARA&A, 54, 529, doi: [10.1146/annurev-astro-081915-023441](https://doi.org/10.1146/annurev-astro-081915-023441)
- Bodaghee, A., Tomsick, J. A., Rodriguez, J., & James, J. B. 2012, ApJ, 744, 108, doi: [10.1088/0004-637X/744/2/108](https://doi.org/10.1088/0004-637X/744/2/108)
- Boumis, P., Mavromatakis, F., & Paleologou, E. V. 2002, A&A, 385, 1042, doi: [10.1051/0004-6361:20020185](https://doi.org/10.1051/0004-6361:20020185)
- Boumis, P., Meaburn, J., López, J. A., et al. 2004, A&A, 424, 583, doi: [10.1051/0004-6361:20040410](https://doi.org/10.1051/0004-6361:20040410)
- Case, G. L., & Bhattacharya, D. 1998, ApJ, 504, 761, doi: [10.1086/306089](https://doi.org/10.1086/306089)
- Caswell, J. L., McClure-Griffiths, N. M., & Cheung, M. C. M. 2004, MNRAS, 352, 1405, doi: [10.1111/j.1365-2966.2004.08030.x](https://doi.org/10.1111/j.1365-2966.2004.08030.x)
- Caswell, J. L., Murray, J. D., Roger, R. S., Cole, D. J., & Cooke, D. J. 1975, A&A, 45, 239
- Cha, A. N., Sembach, K. R., & Danks, A. C. 1999, ApJL, 515, L25, doi: [10.1086/311968](https://doi.org/10.1086/311968)
- Chamba, N., Trujillo, I., & Knapen, J. H. 2020, A&A, 633, L3, doi: [10.1051/0004-6361/201936821](https://doi.org/10.1051/0004-6361/201936821)
- Ciotti, L. 1991, A&A, 249, 99
- Ciotti, L., & Bertin, G. 1999, A&A, 352, 447, <https://arxiv.org/abs/astro-ph/9911078>
- Combi, J. A., Benaglia, P., Romero, G. E., & Sugizaki, M. 2005, A&A, 431, L9, doi: [10.1051/0004-6361:200400136](https://doi.org/10.1051/0004-6361:200400136)
- Corbel, S., Chapuis, C., Dame, T. M., & Durouchoux, P. 1999, ApJL, 526, L29, doi: [10.1086/312359](https://doi.org/10.1086/312359)
- Devin, J., Lemoine-Goumard, M., Grondin, M. H., et al. 2020, A&A, 643, A28, doi: [10.1051/0004-6361/202038503](https://doi.org/10.1051/0004-6361/202038503)
- Dingel, B., Neuhäuser, R., Yerli, S. K., et al. 2015, MNRAS, 448, 3196, doi: [10.1093/mnras/stv124](https://doi.org/10.1093/mnras/stv124)
- Doherty, M., Johnston, S., Green, A. J., et al. 2003, MNRAS, 339, 1048, doi: [10.1046/j.1365-8711.2003.06265.x](https://doi.org/10.1046/j.1365-8711.2003.06265.x)
- Dokara, R., Roy, N., Beuther, H., et al. 2018, ApJ, 866, 61, doi: [10.3847/1538-4357/aadc0c](https://doi.org/10.3847/1538-4357/aadc0c)
- Driessen, L. N., Domček, V., Vink, J., et al. 2018, ApJ, 860, 133, doi: [10.3847/1538-4357/aac32e](https://doi.org/10.3847/1538-4357/aac32e)
- Eger, P., Rowell, G., Kawamura, A., et al. 2011, A&A, 526, A82, doi: [10.1051/0004-6361/201015727](https://doi.org/10.1051/0004-6361/201015727)
- Ferrand, G., & Safi-Harb, S. 2012, Advances in Space Research, 49, 1313, doi: [10.1016/j.asr.2012.02.004](https://doi.org/10.1016/j.asr.2012.02.004)
- Fesen, R. A., & Milisavljevic, D. 2010, AJ, 140, 1163, doi: [10.1088/0004-6256/140/5/1163](https://doi.org/10.1088/0004-6256/140/5/1163)
- Fesen, R. A., Weil, K. E., Cisneros, I. A., Blair, W. P., & Raymond, J. C. 2018, MNRAS, 481, 1786, doi: [10.1093/mnras/sty2370](https://doi.org/10.1093/mnras/sty2370)
- Fesen, R. A., Weil, K. E., Raymond, J. C., et al. 2020, MNRAS, 498, 5194, doi: [10.1093/mnras/staa2765](https://doi.org/10.1093/mnras/staa2765)
- Foster, T., & Routledge, D. 2003, ApJ, 598, 1005, doi: [10.1086/378947](https://doi.org/10.1086/378947)
- Foster, T. J., Cooper, B., Reich, W., Kothes, R., & West, J. 2013, A&A, 549, A107, doi: [10.1051/0004-6361/201220362](https://doi.org/10.1051/0004-6361/201220362)
- Frail, D. A. 2011, Mem. Soc. Astron. Italiana, 82, 703, <https://arxiv.org/abs/1108.4137>
- Frail, D. A., Goss, W. M., Reynoso, E. M., et al. 1996, AJ, 111, 1651, doi: [10.1086/117904](https://doi.org/10.1086/117904)
- Frail, D. A., Goss, W. M., & Whiteoak, J. B. Z. 1994a, ApJ, 437, 781, doi: [10.1086/175038](https://doi.org/10.1086/175038)
- Frail, D. A., Kassim, N. E., & Weiler, K. W. 1994b, AJ, 107, 1120, doi: [10.1086/116923](https://doi.org/10.1086/116923)
- Fraser, M., & Boubert, D. 2019, ApJ, 871, 92, doi: [10.3847/1538-4357/aaf6b8](https://doi.org/10.3847/1538-4357/aaf6b8)
- Fukui, Y., Moriguchi, Y., Tamura, K., et al. 2003, PASJ, 55, L61, doi: [10.1093/pasj/55.5.L61](https://doi.org/10.1093/pasj/55.5.L61)

- Gaensler, B. M., Brazier, K. T. S., Manchester, R. N., Johnston, S., & Green, A. J. 1999, MNRAS, 305, 724, doi: [10.1046/j.1365-8711.1999.02500.x](https://doi.org/10.1046/j.1365-8711.1999.02500.x)
- Gaensler, B. M., Dickel, J. R., & Green, A. J. 2000, ApJ, 542, 380, doi: [10.1086/309522](https://doi.org/10.1086/309522)
- Gaensler, B. M., Manchester, R. N., & Green, A. J. 1998, MNRAS, 296, 813, doi: [10.1046/j.1365-8711.1998.01387.x](https://doi.org/10.1046/j.1365-8711.1998.01387.x)
- Gaensler, B. M., & Wallace, B. J. 2003, ApJ, 594, 326, doi: [10.1086/376861](https://doi.org/10.1086/376861)
- Gao, X. Y., Reich, P., Reich, W., Hou, L. G., & Han, J. L. 2020, MNRAS, 493, 2188, doi: [10.1093/mnras/staa419](https://doi.org/10.1093/mnras/staa419)
- Gao, X. Y., Sun, X. H., Han, J. L., et al. 2011, A&A, 532, A144, doi: [10.1051/0004-6361/201117179](https://doi.org/10.1051/0004-6361/201117179)
- Giacani, E., Smith, M. J. S., Dubner, G., & Loiseau, N. 2011, A&A, 531, A138, doi: [10.1051/0004-6361/201116768](https://doi.org/10.1051/0004-6361/201116768)
- Giacani, E., Smith, M. J. S., Dubner, G., et al. 2009, A&A, 507, 841, doi: [10.1051/0004-6361/200912253](https://doi.org/10.1051/0004-6361/200912253)
- Giacani, E. B., Dubner, G., Cappa, C., & Testori, J. 1998, A&AS, 133, 61, doi: [10.1051/aas:1998310](https://doi.org/10.1051/aas:1998310)
- Giacani, E. B., Dubner, G. M., Green, A. J., Goss, W. M., & Gaensler, B. M. 2000, AJ, 119, 281, doi: [10.1086/301173](https://doi.org/10.1086/301173)
- Gotthelf, E. V., & Halpern, J. P. 2009, ApJL, 700, L158, doi: [10.1088/0004-637X/700/2/L158](https://doi.org/10.1088/0004-637X/700/2/L158)
- Graham, A. W., & Driver, S. P. 2005, PASA, 22, 118, doi: [10.1071/AS05001](https://doi.org/10.1071/AS05001)
- Green, D. A. 1991, PASP, 103, 209, doi: [10.1086/132810](https://doi.org/10.1086/132810)
- . 2004, Bulletin of the Astronomical Society of India, 32, 335. <https://arxiv.org/abs/astro-ph/0411083>
- . 2005, Mem. Soc. Astron. Italiana, 76, 534. <https://arxiv.org/abs/astro-ph/0505428>
- . 2019, Journal of Astrophysics and Astronomy, 40, 36, doi: [10.1007/s12036-019-9601-6](https://doi.org/10.1007/s12036-019-9601-6)
- Hayato, A., Yamaguchi, H., Tamagawa, T., et al. 2010, ApJ, 725, 894, doi: [10.1088/0004-637X/725/1/894](https://doi.org/10.1088/0004-637X/725/1/894)
- Heinz, S., Burton, M., Braiding, C., et al. 2015, ApJ, 806, 265, doi: [10.1088/0004-637X/806/2/265](https://doi.org/10.1088/0004-637X/806/2/265)
- Hessels, J. W. T., Roberts, M. S. E., Ransom, S. M., et al. 2004, ApJ, 612, 389, doi: [10.1086/422408](https://doi.org/10.1086/422408)
- Hewitt, J. W., & Yusef-Zadeh, F. 2009, ApJL, 694, L16, doi: [10.1088/0004-637X/694/1/L16](https://doi.org/10.1088/0004-637X/694/1/L16)
- Hofverberg, P., Chaves, R. C. G., Fiasson, A., et al. 2010, in 25th Texas Symposium on Relativistic Astrophysics, ed. F. M. Rieger, C. van Eldik, & W. Hofmann, 196
- How, T. G., Fesen, R. A., Neustadt, J. M. M., Black, C. S., & Outters, N. 2018, MNRAS, 478, 1987, doi: [10.1093/mnras/sty1007](https://doi.org/10.1093/mnras/sty1007)
- Huang, R. H. H., Wu, J. H. K., Hui, C. Y., et al. 2014, ApJ, 785, 118, doi: [10.1088/0004-637X/785/2/118](https://doi.org/10.1088/0004-637X/785/2/118)
- Hurley-Walker, N., Filipović, M. D., Gaensler, B. M., et al. 2019, PASA, 36, e045, doi: [10.1017/pasa.2019.34](https://doi.org/10.1017/pasa.2019.34)
- Jackson, M. S., Safi-Harb, S., Kothes, R., & Foster, T. 2008, ApJ, 674, 936, doi: [10.1086/524098](https://doi.org/10.1086/524098)
- Jeong, I.-G., Koo, B.-C., Cho, W.-K., et al. 2013, ApJ, 770, 105, doi: [10.1088/0004-637X/770/2/105](https://doi.org/10.1088/0004-637X/770/2/105)
- Kang, J.-h., Koo, B.-C., & Salter, C. 2012, AJ, 143, 75, doi: [10.1088/0004-6256/143/3/75](https://doi.org/10.1088/0004-6256/143/3/75)
- Kargaltsev, O., & Pavlov, G. G. 2010, in American Institute of Physics Conference Series, Vol. 1248, X-ray Astronomy 2009; Present Status, Multi-Wavelength Approach and Future Perspectives, ed. A. Comastri, L. Angelini, & M. Cappi, 25–28
- Karpova, A., Shternin, P., Zyuzin, D., Danilenko, A., & Shibanov, Y. 2016, MNRAS, 462, 3845, doi: [10.1093/mnras/stw1898](https://doi.org/10.1093/mnras/stw1898)
- Kassim, N. E., & Frail, D. A. 1996, MNRAS, 283, L51, doi: [10.1093/mnras/283.3.L51](https://doi.org/10.1093/mnras/283.3.L51)
- Katsuda, S., Tanaka, M., Morokuma, T., Fesen, R., & Milisavljevic, D. 2016, ApJ, 826, 108, doi: [10.3847/0004-637X/826/2/108](https://doi.org/10.3847/0004-637X/826/2/108)
- Kilpatrick, C. D., Bieging, J. H., & Rieke, G. H. 2016, ApJ, 816, 1, doi: [10.3847/0004-637X/816/1/1](https://doi.org/10.3847/0004-637X/816/1/1)
- Kim, I. J., Min, K. W., Seon, K. I., Han, W., & Edelstein, J. 2010, ApJ, 709, 823, doi: [10.1088/0004-637X/709/2/823](https://doi.org/10.1088/0004-637X/709/2/823)
- Kodaira, K. 1974, PASJ, 26, 255
- Koralesky, B., Frail, D. A., Goss, W. M., Claussen, M. J., & Green, A. J. 1998, AJ, 116, 1323, doi: [10.1086/300508](https://doi.org/10.1086/300508)
- Kothes, R. 2003, A&A, 408, 187, doi: [10.1051/0004-6361:20030853](https://doi.org/10.1051/0004-6361:20030853)
- . 2013, A&A, 560, A18, doi: [10.1051/0004-6361/201219839](https://doi.org/10.1051/0004-6361/201219839)
- Kothes, R., & Dougherty, S. M. 2007, A&A, 468, 993, doi: [10.1051/0004-6361:20077309](https://doi.org/10.1051/0004-6361:20077309)
- Kothes, R., Landecker, T. L., Reich, W., Safi-Harb, S., & Arzoumanian, Z. 2008, ApJ, 687, 516, doi: [10.1086/591653](https://doi.org/10.1086/591653)
- Kothes, R., Reich, P., Foster, T. J., & Reich, W. 2017, A&A, 597, A116, doi: [10.1051/0004-6361/201629848](https://doi.org/10.1051/0004-6361/201629848)
- Kothes, R., Reich, W., Foster, T., & Byun, D.-Y. 2003, ApJ, 588, 852, doi: [10.1086/374219](https://doi.org/10.1086/374219)
- Kothes, R., Sun, X. H., Reich, W., & Foster, T. J. 2014, ApJL, 784, L26, doi: [10.1088/2041-8205/784/2/L26](https://doi.org/10.1088/2041-8205/784/2/L26)
- Kothes, R., Uyaniker, B., & Pineault, S. 2001, ApJ, 560, 236, doi: [10.1086/322511](https://doi.org/10.1086/322511)
- Kothes, R., Uyaniker, B., & Reid, R. I. 2005, A&A, 444, 871, doi: [10.1051/0004-6361:20053831](https://doi.org/10.1051/0004-6361:20053831)
- Leahy, D., & Tian, W. 2006, A&A, 451, 251, doi: [10.1051/0004-6361:20054661](https://doi.org/10.1051/0004-6361:20054661)

- Leahy, D. A., Green, K., & Ranasinghe, S. 2013, MNRAS, 436, 968, doi: [10.1093/mnras/stt1596](https://doi.org/10.1093/mnras/stt1596)
- Leahy, D. A., & Green, K. S. 2012, ApJ, 760, 25, doi: [10.1088/0004-637X/760/1/25](https://doi.org/10.1088/0004-637X/760/1/25)
- Leahy, D. A., Nousek, J., & Hamilton, A. J. S. 1991, ApJ, 374, 218, doi: [10.1086/170111](https://doi.org/10.1086/170111)
- Leahy, D. A., & Ranasinghe, S. 2012, MNRAS, 423, 718, doi: [10.1111/j.1365-2966.2012.20909.x](https://doi.org/10.1111/j.1365-2966.2012.20909.x)
- Leahy, D. A., & Tian, W. W. 2007, A&A, 461, 1013, doi: [10.1051/0004-6361:20065895](https://doi.org/10.1051/0004-6361:20065895)
- Leahy, D. A., & Wu, X. 1989, PASP, 101, 607, doi: [10.1086/132475](https://doi.org/10.1086/132475)
- Liszt, H. S. 2009, A&A, 508, 1331, doi: [10.1051/0004-6361/200912421](https://doi.org/10.1051/0004-6361/200912421)
- Lockman, F. J. 1981, ApJ, 245, 459, doi: [10.1086/158822](https://doi.org/10.1086/158822)
- Lorimer, D. R., & Xilouris, K. M. 2000, ApJ, 545, 385, doi: [10.1086/317815](https://doi.org/10.1086/317815)
- Lucy, L. B. 2000, MNRAS, 318, 92, doi: [10.1046/j.1365-8711.2000.03655.x](https://doi.org/10.1046/j.1365-8711.2000.03655.x)
- Matthews, B. C., Wallace, B. J., & Taylor, A. R. 1998, ApJ, 493, 312, doi: [10.1086/305112](https://doi.org/10.1086/305112)
- Maxted, N. I., Braiding, C., Wong, G. F., et al. 2018, MNRAS, 480, 134, doi: [10.1093/mnras/sty1797](https://doi.org/10.1093/mnras/sty1797)
- McClure-Griffiths, N. M., Green, A. J., Dickey, J. M., et al. 2001, ApJ, 551, 394, doi: [10.1086/320095](https://doi.org/10.1086/320095)
- McCullough, P. R., Fields, B. D., & Pavlidou, V. 2002, ApJL, 576, L41, doi: [10.1086/343100](https://doi.org/10.1086/343100)
- Milne, D. K., Roger, R. S., Kesteven, M. J., et al. 1986, MNRAS, 223, 487, doi: [10.1093/mnras/223.3.487](https://doi.org/10.1093/mnras/223.3.487)
- Minami, S., Ota, N., Yamauchi, S., & Koyama, K. 2013, PASJ, 65, 99, doi: [10.1093/pasj/65.5.99](https://doi.org/10.1093/pasj/65.5.99)
- Petriella, A. 2019, A&A, 626, A65, doi: [10.1051/0004-6361/201834734](https://doi.org/10.1051/0004-6361/201834734)
- Pihlström, Y. M., Sjouwerman, L. O., Frail, D. A., et al. 2014, AJ, 147, 73, doi: [10.1088/0004-6256/147/4/73](https://doi.org/10.1088/0004-6256/147/4/73)
- Pineault, S., Landecker, T. L., Madore, B., & Gaumont-Guay, S. 1993, AJ, 105, 1060, doi: [10.1086/116493](https://doi.org/10.1086/116493)
- Press, W. H., Teukolsky, S. A., Vetterling, W. T., & Flannery, B. P. 2007, Numerical Recipes 3rd Edition: The Art of Scientific Computing, 3rd edn. (Cambridge University Press). http://www.amazon.com/Numerical-Recipes-3rd-Scientific-Computing/dp/0521880688/ref=sr_1_1?ie=UTF8&s=books&qid=1280322496&sr=8-1
- Prinz, T., & Becker, W. 2013, A&A, 550, A33, doi: [10.1051/0004-6361/201220297](https://doi.org/10.1051/0004-6361/201220297)
- Rakowski, C. E., Badenes, C., Gaensler, B. M., et al. 2006, ApJ, 646, 982, doi: [10.1086/505018](https://doi.org/10.1086/505018)
- Ranasinghe, S., Leahy, D., & Stil, J. 2021, Universe, 7, 338, doi: [10.3390/universe7090338](https://doi.org/10.3390/universe7090338)
- Ranasinghe, S., Leahy, D., & Tian, W. W. 2020, Journal of High Energy Physics, Gravitation and Cosmology, 6, 9, doi: [10.4236/jhepgc.202061002](https://doi.org/10.4236/jhepgc.202061002)
- Ranasinghe, S., & Leahy, D. A. 2017, ApJ, 843, 119, doi: [10.3847/1538-4357/aa7894](https://doi.org/10.3847/1538-4357/aa7894)
- . 2018a, MNRAS, 477, 2243, doi: [10.1093/mnras/sty817](https://doi.org/10.1093/mnras/sty817)
- . 2018b, AJ, 155, 204, doi: [10.3847/1538-3881/aab9be](https://doi.org/10.3847/1538-3881/aab9be)
- Ranasinghe, S., Leahy, D. A., & Tian, W. 2018, Open Physics Journal, 4, 1, doi: [10.2174/1874843001804010001](https://doi.org/10.2174/1874843001804010001)
- Reid, M. J. 1993, ARA&A, 31, 345, doi: [10.1146/annurev.aa.31.090193.002021](https://doi.org/10.1146/annurev.aa.31.090193.002021)
- Reid, M. J., Menten, K. M., Brunthaler, A., et al. 2014, ApJ, 783, 130, doi: [10.1088/0004-637X/783/2/130](https://doi.org/10.1088/0004-637X/783/2/130)
- Renaud, M., Marandon, V., Gotthelf, E. V., et al. 2010, ApJ, 716, 663, doi: [10.1088/0004-637X/716/1/663](https://doi.org/10.1088/0004-637X/716/1/663)
- Reynolds, S. P., Borkowski, K. J., Green, D. A., et al. 2008, ApJL, 680, L41, doi: [10.1086/589570](https://doi.org/10.1086/589570)
- Reynoso, E. M., Cichowolski, S., & Walsh, A. J. 2017, MNRAS, 464, 3029, doi: [10.1093/mnras/stw2219](https://doi.org/10.1093/mnras/stw2219)
- Reynoso, E. M., Johnston, S., Green, A. J., & Koribalski, B. S. 2006, MNRAS, 369, 416, doi: [10.1111/j.1365-2966.2006.10325.x](https://doi.org/10.1111/j.1365-2966.2006.10325.x)
- Roberts, M. S. E., & Brogan, C. L. 2008, ApJ, 681, 320, doi: [10.1086/588419](https://doi.org/10.1086/588419)
- Roger, R. S., Milne, D. K., Caswell, J. L., & Little, A. G. 1986, MNRAS, 219, 815, doi: [10.1093/mnras/219.4.815](https://doi.org/10.1093/mnras/219.4.815)
- Rosado, M., Ambrocio-Cruz, P., Le Coarer, E., & Marcelin, M. 1996, A&A, 315, 243
- Roy, S., & Pal, S. 2013, ApJ, 774, 150, doi: [10.1088/0004-637X/774/2/150](https://doi.org/10.1088/0004-637X/774/2/150)
- Russeil, D. 2003, A&A, 397, 133, doi: [10.1051/0004-6361:20021504](https://doi.org/10.1051/0004-6361:20021504)
- Sánchez-Cruces, M., Rosado, M., Fuentes-Carrera, I., & Ambrocio-Cruz, P. 2018, MNRAS, 473, 1705, doi: [10.1093/mnras/stx2460](https://doi.org/10.1093/mnras/stx2460)
- Sankrit, R., Raymond, J. C., Blair, W. P., et al. 2016, ApJ, 817, 36, doi: [10.3847/0004-637X/817/1/36](https://doi.org/10.3847/0004-637X/817/1/36)
- Sarma, A. P., Goss, W. M., Green, A. J., & Frail, D. A. 1997, ApJ, 483, 335, doi: [10.1086/304246](https://doi.org/10.1086/304246)
- Sawada, M., Tachibana, K., Uchida, H., et al. 2019, PASJ, 71, 61, doi: [10.1093/pasj/psz036](https://doi.org/10.1093/pasj/psz036)
- Sérscic, J. L. 1963, Boletin de la Asociacion Argentina de Astronomia La Plata Argentina, 6, 41
- Seward, F. D., Dame, T. M., Fesen, R. A., & Aschenbach, B. 1995, ApJ, 449, 681, doi: [10.1086/176089](https://doi.org/10.1086/176089)
- Sezer, A., & Gök, F. 2012, MNRAS, 421, 3538, doi: [10.1111/j.1365-2966.2012.20570.x](https://doi.org/10.1111/j.1365-2966.2012.20570.x)

- Shan, S.-S., Zhu, H., Tian, W.-W., et al. 2019, Research in Astronomy and Astrophysics, 19, 092, doi: [10.1088/1674-4527/19/7/92](https://doi.org/10.1088/1674-4527/19/7/92)
- Shan, S. S., Zhu, H., Tian, W. W., et al. 2018, ApJS, 238, 35, doi: [10.3847/1538-4365/aae07a](https://doi.org/10.3847/1538-4365/aae07a)
- Shen, J., & Zheng, X.-W. 2020, Research in Astronomy and Astrophysics, 20, 159, doi: [10.1088/1674-4527/20/10/159](https://doi.org/10.1088/1674-4527/20/10/159)
- Sparke, L. S., & Gallagher, John S., I. 2007, Galaxies in the Universe: An Introduction
- Stecker, F. W., & Jones, F. C. 1977, ApJ, 217, 843, doi: [10.1086/155631](https://doi.org/10.1086/155631)
- Stupar, M., Parker, Q. A., & Filipović, M. D. 2007, MNRAS, 374, 1441, doi: [10.1111/j.1365-2966.2006.11248.x](https://doi.org/10.1111/j.1365-2966.2006.11248.x)
- Su, H.-Q., Zhang, M.-F., Zhu, H., & Wu, D. 2017a, Research in Astronomy and Astrophysics, 17, 109, doi: [10.1088/1674-4527/17/10/109](https://doi.org/10.1088/1674-4527/17/10/109)
- Su, Y., Zhou, X., Yang, J., et al. 2017b, ApJ, 845, 48, doi: [10.3847/1538-4357/aa7f2a](https://doi.org/10.3847/1538-4357/aa7f2a)
- . 2018, ApJ, 863, 103, doi: [10.3847/1538-4357/aad04e](https://doi.org/10.3847/1538-4357/aad04e)
- Sun, M., Wang, Z.-r., & Chen, Y. 1999, ApJ, 511, 274, doi: [10.1086/306656](https://doi.org/10.1086/306656)
- Supan, L., Castelletti, G., Peters, W. M., & Kassim, N. E. 2018, A&A, 616, A98, doi: [10.1051/0004-6361/201832995](https://doi.org/10.1051/0004-6361/201832995)
- Supan, L., Supanitsky, A. D., & Castelletti, G. 2016, A&A, 589, A51, doi: [10.1051/0004-6361/201527962](https://doi.org/10.1051/0004-6361/201527962)
- Tammann, G. A., Loeffler, W., & Schroeder, A. 1994, ApJS, 92, 487, doi: [10.1086/192002](https://doi.org/10.1086/192002)
- Tian, W. W., Havercorn, M., & Zhang, H. Y. 2007a, MNRAS, 378, 1283, doi: [10.1111/j.1365-2966.2007.11613.x](https://doi.org/10.1111/j.1365-2966.2007.11613.x)
- Tian, W. W., & Leahy, D. A. 2006a, A&A, 455, 1053, doi: [10.1051/0004-6361:20065140](https://doi.org/10.1051/0004-6361:20065140)
- . 2006b, A&A, 447, 205, doi: [10.1051/0004-6361:20054036](https://doi.org/10.1051/0004-6361:20054036)
- . 2012, MNRAS, 421, 2593, doi: [10.1111/j.1365-2966.2012.20491.x](https://doi.org/10.1111/j.1365-2966.2012.20491.x)
- . 2014, ApJL, 783, L2, doi: [10.1088/2041-8205/783/1/L2](https://doi.org/10.1088/2041-8205/783/1/L2)
- Tian, W. W., Leahy, D. A., & Foster, T. J. 2007b, A&A, 465, 907, doi: [10.1051/0004-6361:20066935](https://doi.org/10.1051/0004-6361:20066935)
- Tian, W. W., Leahy, D. A., Havercorn, M., & Jiang, B. 2008, ApJL, 679, L85, doi: [10.1086/589506](https://doi.org/10.1086/589506)
- Tian, W. W., Zhu, H., Zhang, M. F., et al. 2019, PASP, 131, 114301, doi: [10.1088/1538-3873/ab35f4](https://doi.org/10.1088/1538-3873/ab35f4)
- Tiengo, A., Vianello, G., Esposito, P., et al. 2010, ApJ, 710, 227, doi: [10.1088/0004-637X/710/1/227](https://doi.org/10.1088/0004-637X/710/1/227)
- Uyaniker, B., Kothes, R., & Brunt, C. M. 2002, ApJ, 565, 1022, doi: [10.1086/324782](https://doi.org/10.1086/324782)
- Velázquez, P. F., Dubner, G. M., Goss, W. M., & Green, A. J. 2002, AJ, 124, 2145, doi: [10.1086/342936](https://doi.org/10.1086/342936)
- Verberne, S., & Vink, J. 2021, MNRAS, 504, 1536, doi: [10.1093/mnras/stab940](https://doi.org/10.1093/mnras/stab940)
- Vink, J. 2004, ApJ, 604, 693, doi: [10.1086/381930](https://doi.org/10.1086/381930)
- Wallace, B. J., Landecker, T. L., & Taylor, A. R. 1997, AJ, 114, 2068, doi: [10.1086/118627](https://doi.org/10.1086/118627)
- Wang, Y., Beuther, H., Rugel, M. R., et al. 2020, A&A, 634, A83, doi: [10.1051/0004-6361/201937095](https://doi.org/10.1051/0004-6361/201937095)
- Wegg, C., Gerhard, O., & Portail, M. 2015, MNRAS, 450, 4050, doi: [10.1093/mnras/stv745](https://doi.org/10.1093/mnras/stv745)
- Welsh, B. Y., Sallmen, S., Jelinsky, S., & Lallement, R. 2003, A&A, 403, 605, doi: [10.1051/0004-6361:20030168](https://doi.org/10.1051/0004-6361:20030168)
- Wilson, A. S. 1986, ApJ, 302, 718, doi: [10.1086/164033](https://doi.org/10.1086/164033)
- Winkler, P. F., Gupta, G., & Long, K. S. 2003, ApJ, 585, 324, doi: [10.1086/345985](https://doi.org/10.1086/345985)
- Xu, J.-L., & Wang, J.-J. 2012, A&A, 543, A24, doi: [10.1051/0004-6361/201219072](https://doi.org/10.1051/0004-6361/201219072)
- Yamauchi, S., Bamba, A., & Koyama, K. 2014, PASJ, 66, 20, doi: [10.1093/pasj/pst021](https://doi.org/10.1093/pasj/pst021)
- Yang, J., Zhang, J.-L., Cai, Z.-Y., Lu, D.-R., & Tan, Y.-H. 2006, ChJA&A, 6, 210, doi: [10.1088/1009-9271/6/2/8](https://doi.org/10.1088/1009-9271/6/2/8)
- Yar-Uyaniker, A., Uyaniker, B., & Kothes, R. 2004, ApJ, 616, 247, doi: [10.1086/424794](https://doi.org/10.1086/424794)
- Yasumi, M., Nobukawa, M., Nakashima, S., et al. 2014, PASJ, 66, 68, doi: [10.1093/pasj/psu043](https://doi.org/10.1093/pasj/psu043)
- Yu, B., Chen, B. Q., Jiang, B. W., & Zijlstra, A. 2019, MNRAS, 488, 3129, doi: [10.1093/mnras/stz1940](https://doi.org/10.1093/mnras/stz1940)
- Zdziarski, A. A., Malyshev, D., de Oña Wilhelmi, E., et al. 2016, MNRAS, 455, 1451, doi: [10.1093/mnras/stv2167](https://doi.org/10.1093/mnras/stv2167)
- Zhou, P., Zhou, X., Chen, Y., et al. 2020a, ApJ, 905, 99, doi: [10.3847/1538-4357/abc34a](https://doi.org/10.3847/1538-4357/abc34a)
- Zhou, X., Su, Y., Yang, J., et al. 2020b, ApJ, 900, 155, doi: [10.3847/1538-4357/aba8fe](https://doi.org/10.3847/1538-4357/aba8fe)
- Zhou, X., Yang, J., Fang, M., et al. 2016, ApJ, 833, 4, doi: [10.3847/0004-637X/833/1/4](https://doi.org/10.3847/0004-637X/833/1/4)
- Zhu, H., Tian, W. W., & Wu, D. 2015, MNRAS, 452, 3470, doi: [10.1093/mnras/stv1534](https://doi.org/10.1093/mnras/stv1534)